Special Publication 20, pp. 379–401

Chapter 18

Geology, Structure, and Radiometric Age Determination of the Murowa Kimberlites, Zimbabwe*

S. Moss,[1,†,**] B. E. Marten,[2] M. Felgate,[3] C. B. Smith,[4] L. Chimuka,[5] E. L. Matchan,[3] and D. Phillips[3]

[1] *Mineral Services Canada, 501 88 Lonsdale Avenue, North Vancouver, British Columbia V7M 2E6, Canada*

[2] *Consulting Geologist, Baltimore, County Cork, Ireland*

[3] *School of Earth Sciences, University of Melbourne, Parkville, Victoria 3010, Australia*

[4] *School of Earth Sciences, University of Bristol, Wills Memorial Building, Queen's Road, Bristol BS8 1RJ, United Kingdom*

[5] *RioZim, Murowa Diamond Mine, Zimbabwe*

Abstract

The Murowa kimberlite field includes three diamondiferous kimberlite pipes (K1, K2, and K3) and multiple kimberlite dikes that have been emplaced into the Archean Chibi granite batholith north of the Limpopo belt in south-central Zimbabwe. Here we summarize the key aspects of the geology of the Murowa kimberlites from previous studies and integrate these findings with new structural data to interpret a structural model governing the locations, relative positions, and orientations of emplaced kimberlite. Key observations of drill core, thin section petrography, geochemistry, and mapping of exposed rocks at the Murowa diamond mine are summarized from previous work, and these data collectively form the basis for emplacement interpretations and three-dimensional (3-D) geologic models of each body. Structural observations are used to interpret the presence of a km-scale tensile bridge hosting the Murowa kimberlites and suggest Murowa is an example of kimberlite emplacement into multiple, reactivated, preexisting near-surface structures at different orientations. We propose that the physical state of the ascending magma (% of gas, extent of phase separation) can dictate whether kimberlite is emplaced along preexisting structures or creates and intrudes new fracture networks in planes of weak horizontal stress. A reproducible age of ~526 Ma is determined for two coherent kimberlite dikes at K1, while an older Rb-Sr model age of ~543 Ma is calculated for a single dike from K2, though this result is of limited reliability due to potential disturbance of the Rb-Sr system due to phlogopite alteration. These results highlight potential problems with reported ages from kimberlite pipes.

Introduction

The Murowa kimberlite field includes three diamondiferous kimberlite pipes (K1, K2, and K3) and multiple kimberlite dikes that were emplaced into the Archean Chibi granite batholith north of the Limpopo belt in south-central Zimbabwe (Fig. 1A, B), and were mined for diamonds by Rio Tinto and RioZim from 2004 to 2015. The exploration history, regional geology, and general character of the Murowa project were first described by Smith et al. (2004) and are further described by Sims et al. (2018). The nature of the underlying mantle and of the Murowa diamonds and their inclusions are described by Pearson et al. (2018) and Bulanova et al. (2018), respectively. Early descriptions of the geology recognized a complex array of textures comprising volcaniclastic kimberlite rocks, coherent kimberlite rocks, variable country rock breccias, and metasomatically altered country rock within and around the Murowa pipes (Smith et al., 2004), and initial geology models were developed for K1, K2, and K3 based on logging of drill cores by Rio Tinto. Subsequent exploration and mining revealed additional breccia and volcaniclastic rock types and allowed for more detailed study of their texture, geometry, spatial associations, and relative timing of emplacement through mapping and review of drill cores, leading to a revision of the internal geology model (Moss et al., 2013).

These studies indicate the pipes at Murowa show apparently contrasting host-rock geology, kimberlite infill, and shapes, and are distinct relative to some other kimberlite pipes due to the extensive occurrence of country-rock breccias with minor (0–20%) kimberlitic components (i.e., olivine, clasts of solidified kimberlite melt), discontinuously around pipe margins and locally as lenses within in situ, unbrecciated country rock. The country rock and country-rock breccias surrounding the kimberlite pipes at Murowa are notable because of evidence of metasomatic alteration of granite to syenite by kimberlitic fluids (Smith et al., 2004), a feature observed to lesser extents around some other kimberlites (e.g., Clement, 1982; Field et al., 1997; Hetman et al., 2004; Fitzgerald et al., 2009).

The updated model pipe geometry was combined with observed crosscutting relationships and textural heterogeneity among the deposits to interpret a range of emplacement styles at Murowa. The apparent complexity at K1 was interpreted to indicate multiple intrusion/eruption events of kimberlite magmas with different proportions of gas, liquids, and solid phases through variable country-rock regimes, with associated thermohydraulic explosion, fracturing, brecciation, and fluidization occurring over contrasting timescales. The K2

† Corresponding author: e-mail, smoss@terramvero.com

*A digital supplement to this paper is available online at www.segweb.org/SP20-Appendices and on the flash drive included with this volume.

**Present address: Terram Vero Consulting Inc., 2685 Dundas Street, Vancouver, BC V5K 1R1, Canada.

doi: 10.5382/SP.20.18; 23 p.

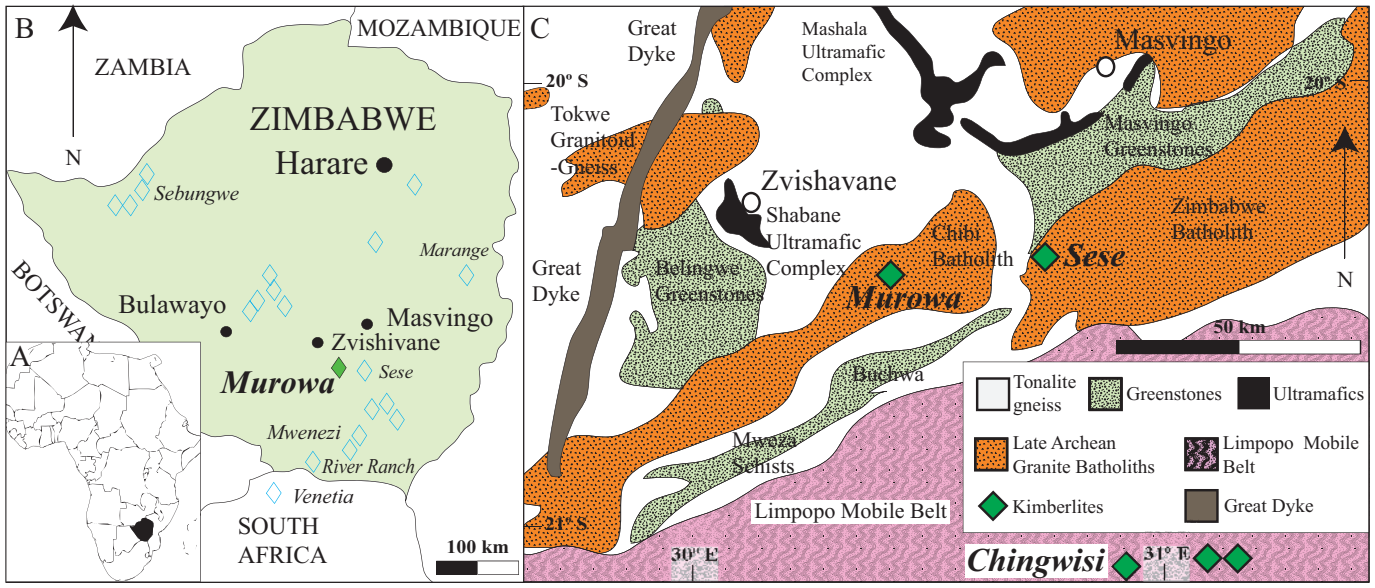

Fig. 1. Maps showing the location of Murowa: A-B) Murowa is located in south-central Zimbabwe, 60 km southeast of Zvishavane. Known diamond occurrences in the region are indicated by open blue diamonds. C) Location of Murowa in relation to geology of the southern margin of the Zimbabwe craton, adjacent to the Limpopo belt. Kimberlite clusters are shown in green. Modified from Moss et al. (2013) and Smith et al. (2004).

pipe was interpreted to reflect a more passive emplacement of coherent kimberlite following early metasomatism and explosive pipe excavation (Moss et al., 2013). Historical structural data from the exploration stages at Murowa were not included in this interpretation, and no age data for the kimberlites were available at the time.

Research on kimberlite emplacement (Helmstaedt, 2018) suggests that the locations and orientations of kimberlite dikes and pipes are in direct response to preexisting structures (Kurszlaukis and Barnett, 2003), are controlled by local structures (e.g., Deakin and White, 1991; White et al., 1995; Jelsma et al., 2004), result from kimberlites intruding their own fracture systems (e.g., Basson and Viola, 2003; Kavanagh, 2010), or are controlled by regional structures dictating a local stress tensor which, in turn, determines the trend of dike emplacement (Barnett et al., 2013). However, a remaining concern is the lack of adequate field studies to substantiate these ideas, and little consideration is given to the spatial and temporal relationships of different kimberlite facies relative to structures and the implications these may have on emplacement location.

We summarize the key aspects of the geology of the Murowa kimberlites from studies to date, present new structural mapping data, and offer the first radiometric age constraints for the Murowa kimberlite cluster. Key observations of drill core, thin section petrography, geochemistry, and mapping of exposed rocks at the Murowa diamond mine are summarized below from previous work (Smith et al., 2004; Moss et al., 2013), and these data collectively form the basis for three-dimensional (3-D) geologic models of each body. Structural field data are used to interpret the presence of a km-scale tensile bridge hosting the Murowa kimberlites and provide a case study showing that, in at least some cases, kimberlite can be emplaced into and reactivate multiple, preexisting near-surface structures at different orientations. We use observations at Murowa to propose that the physical state of the ascending magma (% of gas, extent of phase separation) can dictate whether kimberlite is emplaced along preexisting structures or creates and intrudes new fracture networks in zones of weak horizontal stress. Ages for coherent kimberlite dikes from K1 and K2 are determined using multiple radiometric dating methods (Rb-Sr, U-Pb, and $^{40}Ar/^{39}Ar$). Although there is overall good agreement between ages calculated via the three techniques, the results highlight the nontrivial task of dating kimberlites and call into question previously reported ages based solely on Rb-Sr data or from samples collected from a single facies within a kimberlite pipe.

Regional Geology

The Murowa area is located near the southeast edge of the Zimbabwe craton, in the foreland of the Limpopo mobile belt (Fig. 1). The nucleus of the Zimbabwe craton is represented by the Shabani Gneiss, a polycyclic tonalitic gneiss complex which stabilized at 3.5 Ga, includes remnants of ancient Sebakwian greenstones, and also formed a continental basement to parts of the Belingwe greenstone belt of the Bulawayan system (Bickle et al., 1994). The northeasterly trending Buhwa greenstone belt lies approximately 15 km to the south of Murowa and hosts a banded iron formation exploited at Buchwa for iron ore up until the late 1980s. The greenstone formations apparent in the Buchwa area were probably established by 2.8 Ga and are contained as remnants within the Mweza schist belt (Hofmann et al., 2001; Fig. 1C). This belt sits on the northern margin of the Limpopo thrust zone and formed as a precursor phase to the Limpopo event. The Shabani Gneiss is cut by the Mashaba-Chibi mafic dikes on east-southeast and east-northeast trends. The Murowa kimberlites intrude the Chibi Granites (2.6 Ga; Luais and Hawkesworth,

1994), which form part of a regional batholithic intrusive event into the basement Shabani Gneisses. The Chibi batholith also truncates the Mashaba-Chibi dikes (Hawkesworth et al., 1979). This batholith is part of the Late Archean Chilimanzi Suite adamellites and forms an elongate pluton about 20 km wide extending east-northeast for about 140 km, parallel to the margin of the Limpopo belt. It is posttectonic with respect to Archean events. The Chibi batholith is cut by two sets of fracture systems that control a trellis-type drainage pattern. The kimberlite field is bounded some 15 km to the north by the Tokwe cratonic segment, which stabilized at about 3.5 Ga.

The Mweza schist belt occurs in a strong ENE-trending lineament that transects the south part of the area and merges into the south margin of the Masvingo greenstone belt. This lineament is at a slight angle to the margin of the Limpopo belt in the Masvingo area, though it is parallel to it in the Buchwa-Mweza area. It appears to be a major sinistral shear belt that was a precursor to the main Limpopo event.

Two features of regional extent are recognizable in the immediate Murowa area. The first is a prominent set of NNE-trending faults and fractures in the Chibi batholith that is part of the sinistral Popoteke strike-slip fault system. This set of fractures is related to the emplacement of the Great Dyke and satellite intrusions such as the East Dyke (Wilson, 1990), and may have developed immediately prior to or synchronously with the 2575.4 ± 0.7 Ma (Soederlund et al., 2010) emplacement of the Great Dyke. The East Dyke, part of the Great Dyke (Fig. 1) ultra-mafic intrusive event (2.4 Ga), lies approximately 50 km to the west of the Murowa site. This event is reflected in the dominant north-northeasterly lineaments in the area, and these structures control much of the structural morphology and trends of the area. The lineaments are generally host to mafic intrusives including picrites. The apparent control exerted by the fractures on the emplacement of the Great Dyke and its satellites indicates that it was a deep, mantle-tapping system of fractures.

The second feature is the Sebanga Poort Dyke, which can be traced discontinuously from the Mweza schist belt through Murowa to the north-northwest for about 300 km (Keep et al., 1970; Robertson, 1974). A dolerite dike, which is a splay of the Sebanga Poort Dyke, lies immediately to the west of Murowa pipes and is part of the Mashonaland dolerite suite, which cut the whole of the Zimbabwe craton at 2408.3 ± 2.0 Ma (Soederlund et al., 2010). The dominant north-northwest trend of the Mashonaland dikes possibly represents the tension gash direction related to regional east-west dextral shear.

Kimberlite Geology of Murowa Pipes

Methods

Geologic data for K1 and K2 reported here were collected through detailed logging of selected drill cores (43 drill holes and 12,000 m for K1; 17 drill holes and 4,900 m for K2), petrographic analysis of representative thin sections (83 for K1; 46 for K2), and mapping of exposed rocks in the open pits at different stages of mine development. Geochemical data derived from sampling carried out by Rio Tinto from 1997 to 2000, and whole-rock major and trace-element analyses were obtained by a combination of X-ray fluorescence (XRF) and AAS by Analabs Pty. Ltd., Perth, Western Australia, using methods further described in Smith et al. (2004). These datasets were integrated and used to define distinct geologic domains within each pipe. The morphology and spatial distribution of the geologic domains were then modeled in Gemcom GEMS™ 3-D modeling software. Rocks are generally described after Scott Smith et al. (2013).

K1

The K1 pipe is an irregular-shaped, elongate and multilobed kimberlite pipe. It is 250 m long in a north-south direction, a maximum of 108 m wide in an east-west direction, and lies ~800 m to the north of K2 (Fig. 2). The K1 pipe infill is internally complex and contains five main kimberlite types (K1-KIMB1 to K1-KIMB5) comprising both volcaniclastic and coherent varieties (Table 1; Figs. 2–5), which are collectively phlogopite bearing, relatively K_2O rich, and generally poor in indicator minerals. Distinct petrographic characteristics of the volcaniclastic rock types at K1 (K1-KIMB2, K1-KIMB4) include (1) the presence of ultrathin rims consisting of phlogopite microphencrysts around some olivine and granite fragments, probably representing cored melt-bearing pyroclasts, (2) the moderate modal abundance of pseudomorphic olivine, (3) the high modal abundance of fresh to partially altered, small (<20 cm) granite xenoliths, and (4) the coarse clinopyroxene and serpentine replacement of olivine grains, which produces distinctive "rims" seen in drill core and exposures (Moss et al., 2013). The textural characteristics of the main pipe-filling volcaniclastic rock type at K1, K1-KIMB4, suggest a classification of Kimberley-type pyroclastic kimberlite (formerly "tuffisitic kimberlite"; Scott Smith et al., 2013) and are notable due to the presence of ubiquitous large (0.1–2 m), irregular to subround brown clasts ("blobs") of coherent kimberlite, which together give the rocks an overall "spotted" appearance. The dominant coherent kimberlite rock type (K1-KIMB1) observed in K1 is characterized by abundant, unbroken ultrafine- to ultracoarse-grained olivine and angular to rounded bleached white and gray country-rock xenoliths (5–10 mm) uniformly distributed in a crystalline groundmass comprising phlogopite, monticellite, relatively fine grained spinel and perovskite, and interstitial serpentine. An additional coherent kimberlite rock type (K1-KIMB5) is distinct due to the presence of minor cored spherical melt-bearing pyroclasts in an otherwise coherent rock texture (Moss et al., 2013).

Multiple kimberlite dikes (K1-KDYKEs; 0.5–3 m in horizontal thickness) classified as macrocrystic phlogopite (± monticellite; ± carbonate) coherent kimberlite crosscut the pipe and surrounding country rock (Table 1; Figs. 2–5) and are, in some places, also crosscut by the pipe. The rocks in K1 contain minor amounts of purple and red garnets, ilmenite, chromite, and, generally, minor amounts of garnet harzburgite and garnet lherzolite mantle xenoliths, with the exception of a peridotite xenolith-rich dike (K1-KDYKE-MX).

A variably thick (5–120 m), "marginal" zone of granite breccias with minor amounts of kimberlite surrounds the pipe (Table 2; Figs. 2–6). These rocks were first described by Smith et al. (2004) as granite metasomatized to syenite or "fenite" (see below) and collectively form a distinct, thick "marginal zone" or envelope surrounding and crosscut by all of the pipe

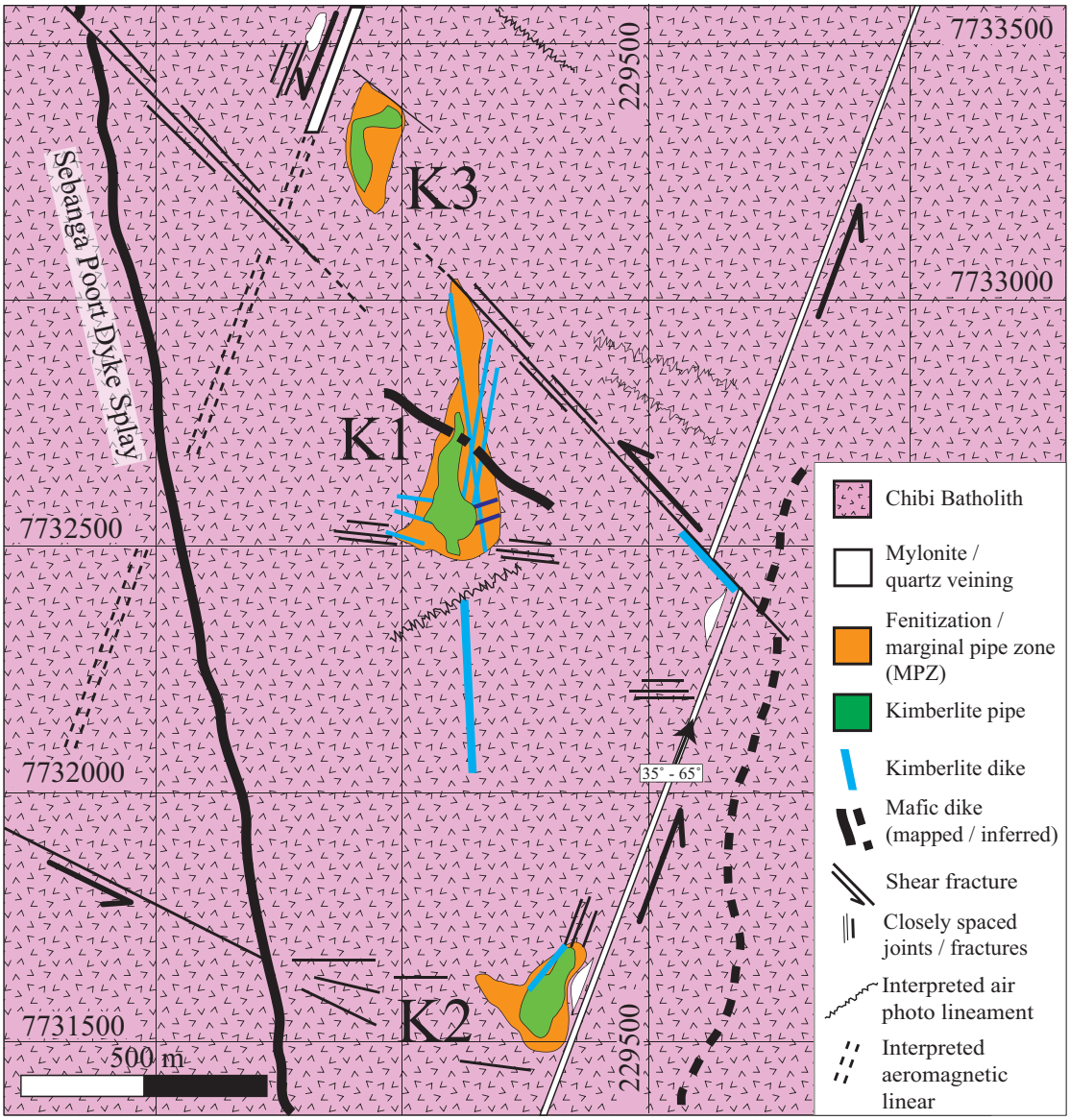

Fig. 2. Local geology map of K1, K2, and K3 and surrounding structural geology of the Murowa area. Kimberlite pipes (green) are each surrounded by a marginal pipe zone (orange) marked by fenitization of granite. Kimberlite dikes are shown in blue; nonkimberlite mafic dikes are in black.

infill, and are thus collectively referred to as the "marginal pipe zone" or K1-MPZ. All rock types in the K1-MPZ contain <20% kimberlitic components (matrix minerals, solid mantle, solidified kimberlite melt), and <3% olivine >1 mm in size, but some occurrences of each rock type do not contain any solid mantle or solidified kimberlite melt. Results from mapping of the rock types from open-pit exposures at K1 are shown in Figures 3 and 6. The rock types comprising the K1 pipe infill and marginal pipe zone are shown in Figures 5 to 7, summarized in Tables 1 and 2, and described more completely in Moss et al. (2013).

K2

K2 is a steep-sided, subcircular, and slightly elongate pipe occurring 800 m south of K1 (Fig. 2). It is 200 m long in a northeast-southwest direction and a maximum of 110 m wide in an east-west direction that flares slightly with depth. Current data suggest the K2 pipe infill is internally simple, being comprised of one main type of coherent kimberlite (K2-KIMB1). Distinct petrographic features of K2-KIMB1 include coarse- to very coarse grained olivine, common extensively altered white granite xenoliths, microphenocrystic phlogopite, and relatively fine grained spinel and perovskite distributed in a groundmass of ultrafine and intergrown phlogopite and less common serpentinized monticellite (Moss et al., 2013). The primary groundmass and, in some cases, also olivine is variably replaced/overprinted by clinopyroxene ± phlogopite ± carbonate ± apatite resulting from the digestion of granite xenoliths. A second volumetrically minor type of coherent kimberlite (K2-KIMB2) is preserved locally near the pipe margins, and is broadly similar to K2-KIMB1, but is distinct due to the coarser grain size and different character

Table 1. Summary of Key Attributes of K1 Kimberlite Rock Types

	K1-KIMB1	K1-KIMB2	K1-KIMB4	K1-KIMB5	K1-KDYKE-MX
Diagnostic features	High % and coarse size of OLV; uniform bleach-white CRX; brown groundmass	Moderate % OLV; high % CRX; alteration rims on OLV	Low-moderate OLV % and heterogeneous distribution; brown CK clasts; high % and varied CRX	Spherical apparent clasts; abundant serp-car "pools" in groundmass	Abundant large peridotite xenoliths
Textural classification	Coherent kimberlite	Volcaniclastic kimberlite	Volcaniclastic kimberlite	Coherent kimberlite	Hypabyssal kimberlite
Mineralogical classification	Phlogopite monticellite	Phlogopite	Phlogopite	Phlogopite	Phlogopite
Hardness	Friable to moderately competent	Competent	Friable to moderately competent	Very hard	Very hard
Color	Brown-gray with black OLV and white CRX	Pale green with pink to gray CRX	Blue-green-gray with brown patches	Black with green-black olivine	Gray-black with black olivine
Dominant structure	Massive at 20- × 20-cm scale	Massive at 20- × 20-cm scale	Massive at 1- × 1-m scale	Massive with local flow banding	Massive with local flow banding and MX concentration
Dominant framework	Groundmass supported	Matrix supported	Matrix supported	Groundmass supported	Groundmass supported
Degree of sorting	Poorly sorted	Poorly sorted	Poorly sorted	Moderately to well sorted	Moderately sorted
Component distribution	Homogeneous	Heterogeneous	Heterogeneous	Homogeneous	Homogeneous
Total olivine abundance (%)	45–60%	15–20%	5–20%	45–55%	25–40%
Olivine size range[1]	vf-vc	vf-c	vf-vc	vf-vc	vf-c
Olivine > 1 mm (%)	25–35%	8–10%	3–15%	25–35%	15–25%
Kimberlite clast abundance	None	1–3%	5–20%	5–8%	None
Kimberlite clast size	Not applicable	<1 cm	1–60 cm	0.5–40 mm	Not applicable
Kimberlite clast type(s)	Not applicable	Cored with ultrathin microlitic phl rims; rare uncored	Cored and uncored; large, irregular blobs Two petrographic types	Cored	Not applicable
Country rock xenolith abundance	8–25%	25–55%	30–70%	0–2%	5–10%
Dominant xenolith types	Granitoid	Granitoid	Granitoid, dolerite, MPZ1, MPZ2a, b	Granitoid	Granitoid
Relative groundmass/ matrix size[1]	Fine	Fine	Very fine	Coarse	Coarse
Groundmass/matrix minerals	Phl, mont; sp, pvk, serp	Cpx, serp, phl	Cpx, serp, phl, car	Car, phl, sp, serp	Phl, sp, car, serp
Mantle xenoliths and xenocrysts	Gnt harz; gnt lherz Ilm and gnt	None observed	Gnt harz; gnt lherz Ilm and gnt	Gnt harz; sp lherz	Sp lherz, gnt harz > gnt lherz

Abbreviations are as follows: car = carbonate, CK = coherent kimberlite, cpx = clinopyroxene, CRX = country rock xenoliths, gnt = garnet, harz = harzburgite, ilm = ilmenite, lherz = lherzolite, mont = monticellite, MX = mantle xenolith, OLV = olivine, phl = phlogopite, pvk = perovskite, serp = serpentine, sp = spinel

[1] Size classes based on Scott-Smith et al. (2013): uf = ultrafine, <0.125 mm; sf = superfine, 0.125–0.25 mm; vvf = very, very fine, >0.25–0.5 mm; vf = very fine, >0.5–1 mm; f = fine, >1–2 mm; m = medium, >2–4 mm; c = coarse, >4–8 mm; vc = very coarse, >8–16 mm; uc = ultracoarse, >16 mm

of groundmass phlogopite and the grain size and character of groundmass spinel. Mantle indicator minerals are rare in K2 and include mauve garnet and spinel, typically present within peridotite microxenoliths.

The country rocks to K2 are variably brecciated and altered granite, syenite, and mylonite with minor quantities of kimberlitic components (0–30%). These rocks form a distinct, thick envelope (20–100 m) around the pipe and are collectively referred to as the "marginal pipe zone" (K2-MPZ), as at K1. The marginal pipe zone at K2 comprises broadly similar rock types, as observed at K1. These variably brecciated and altered rocks contain 0 to 15% kimberlitic components (solid mantle xenoliths or xenocrysts, solidified kimberlite melt, groundmass/matrix minerals) in the form of melt-free olivine grains and, in rare cases, also olivine-poor clasts of solidified kimberlite melt. Late-stage kimberlite dikes crosscut the pipe (K2-KDYKE-INT) and the surrounding K2-MPZ (K2-KDYKE-EXT) and can be further subdivided into two types based on petrography. The rock types comprising the K2 pipe infill and marginal pipe zone are shown in Figure 8, summarized in Table 3, and described more completely in Moss et al. (2013).

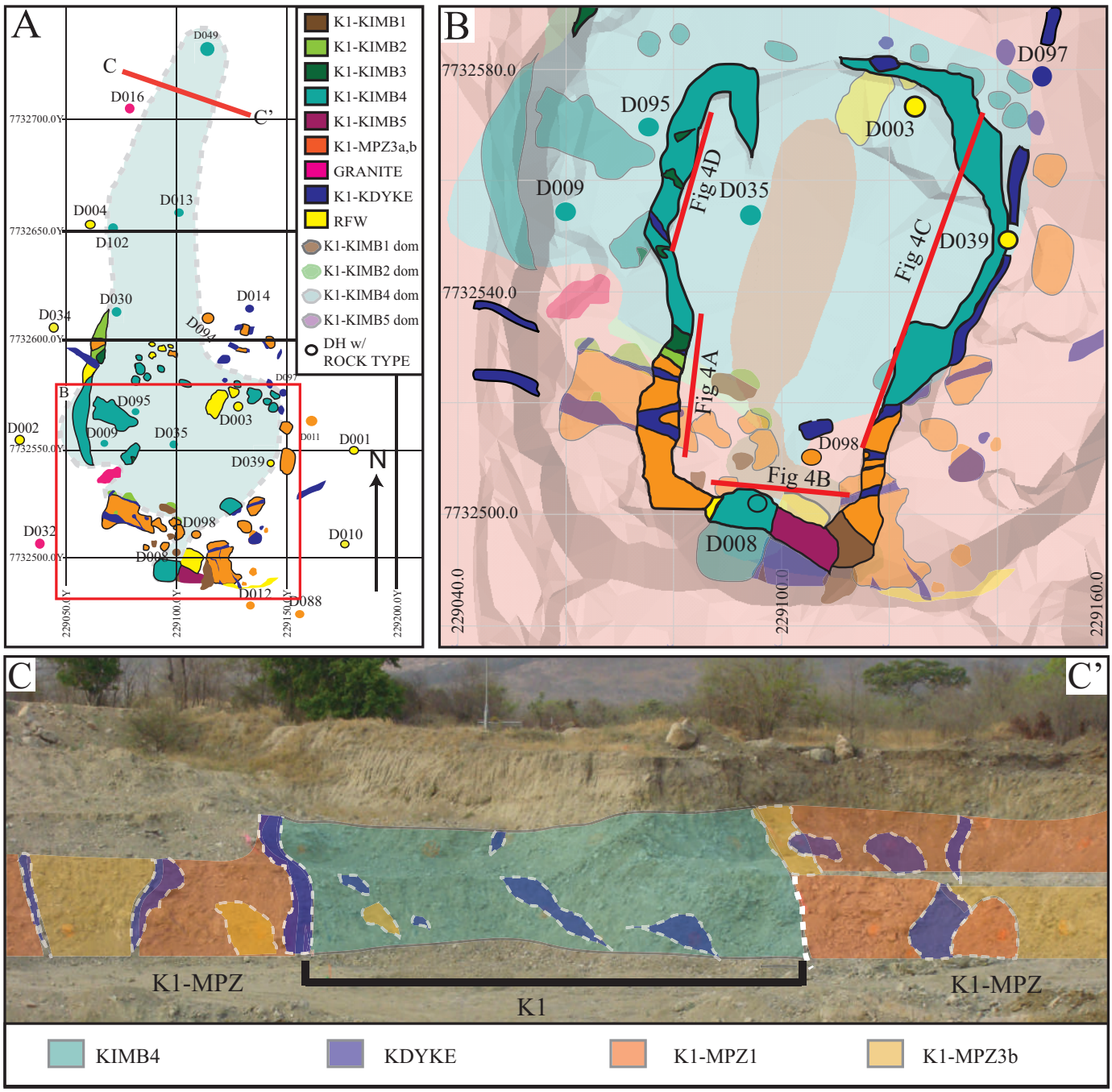

Fig. 3. Mapping of kimberlite deposits at K1. Open-pit mapping of K1 at Murowa: A) Plan view of K1 showing mapped outcrops at 730 to 755 m above sea level (masl) of the various distinct rock types (solid colors): K1-KIMB1 = coherent kimberlite, K1-KIMB2 = volcaniclastic kimberlite, K1-KIMB3 = coherent kimberlite, K1-KIMB4 = volcaniclastic kimberlite, K1-KIMB5 = coherent kimberlite, K1-KDYKE = hypabyssal kimberlite, K1-MPZ3a, b = marginal pipe zone types, GRANITE = in situ, unaltered granite, and RFW = requires further work. Red box indicates area presented in (B) and C-C' indicates cross section for (C). B) Geology map showing outcrops in southern end of K1 at 725 to 730 masl in the open pit. Mapping shown in (A) is made semitransparent, and main pipe-filling kimberlite model domains and pit topography are shown as transparent background. Red lines indicate planes of photographs in Figure 4A to D. C) Profile view of northern limb of K1 at 735 to 745 masl in the open pit showing distribution of mapped rock types in K1 pipe and the marginal pipe zone (MPZ) as semitransparent overlay. Modified from Moss et al. (2013).

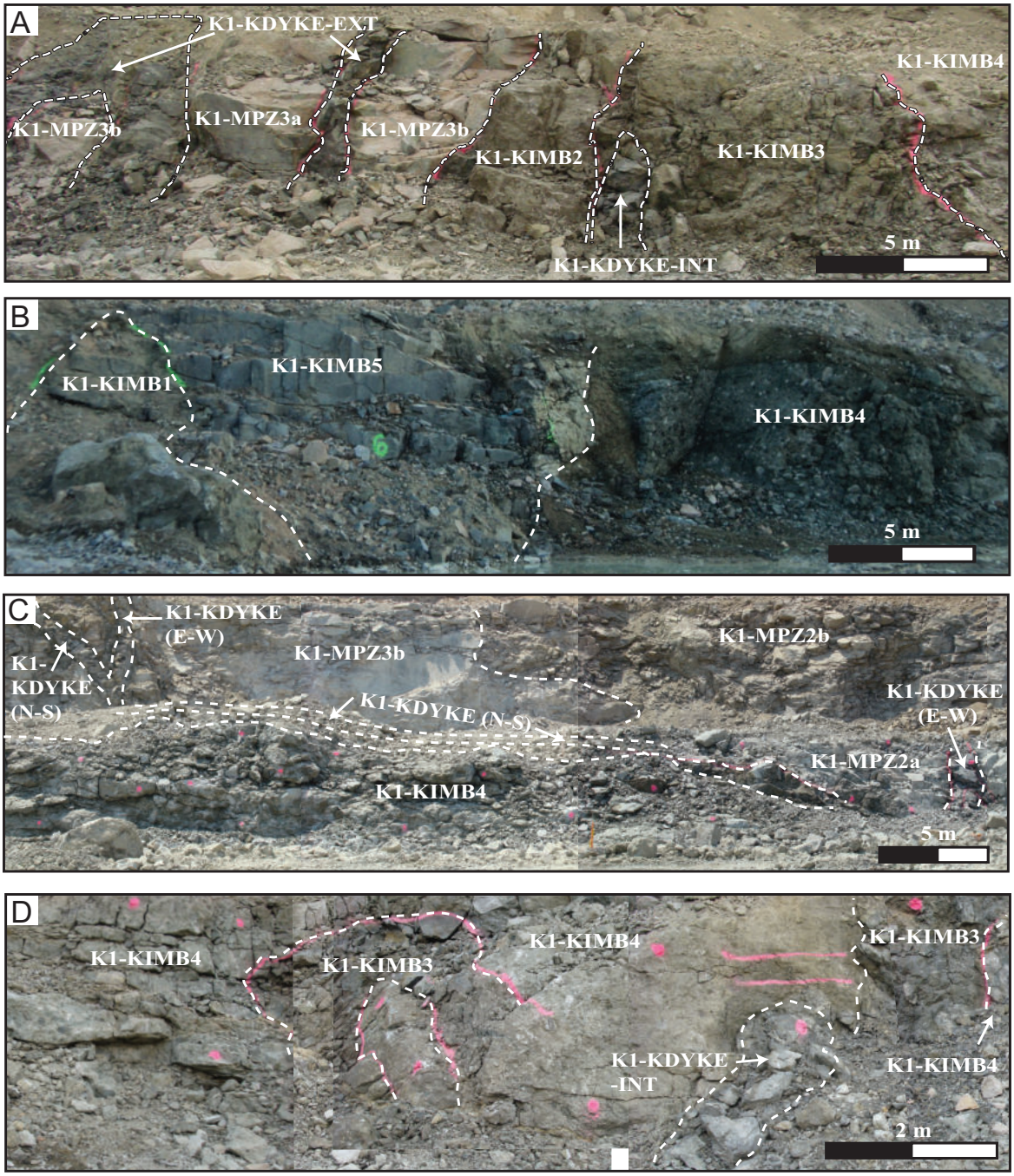

Fig. 4. Photographs from the open pit of K1: A) 5-m wall in the southwest of K1 (photograph taken facing west; wall azimuth ~005°) showing contacts between common rock types K1-MPZ3a, b (marginal pipe zone types), K1-KDYKE-EXT/INT (coherent kimberlite), K1-KIMB3 (volcaniclastic kimberlite), and K1-KIMB4 (volcaniclastic kimberlite). B) Photograph of 10-m wall in the south of K1 (photograph taken facing south; wall azimuth 095°) showing contacts between K1-KIMB1 (coherent kimberlite), K1-KIMB5 (coherent kimberlite), and K1-KIMB4 (volcaniclastic kimberlite). C) Photographs of 5-m (foreground) and 10-m wall (background) in the east of K1 (photograph taken facing east; wall azimuth ~005°) showing contacts between K1-KIMB4, K1-KDYKE, K1-MPZ2a, b, and K1-MPZ3b. KDYKE is indicated as N-S striking (K1-KDYKE [N-S]) and as E-W striking (K1-KDYKE [E-W]). D) Photographs of 5-m wall in the west of K1 (photograph taken facing west; wall azimuth 352°) showing contacts between K1-KIMB4 (volcaniclastic kimberlite), K1-KIMB3 (volcaniclastic kimberlite), and K1-KDYKE-INT (coherent kimberlite). White dashed lines indicate contacts between rock types.

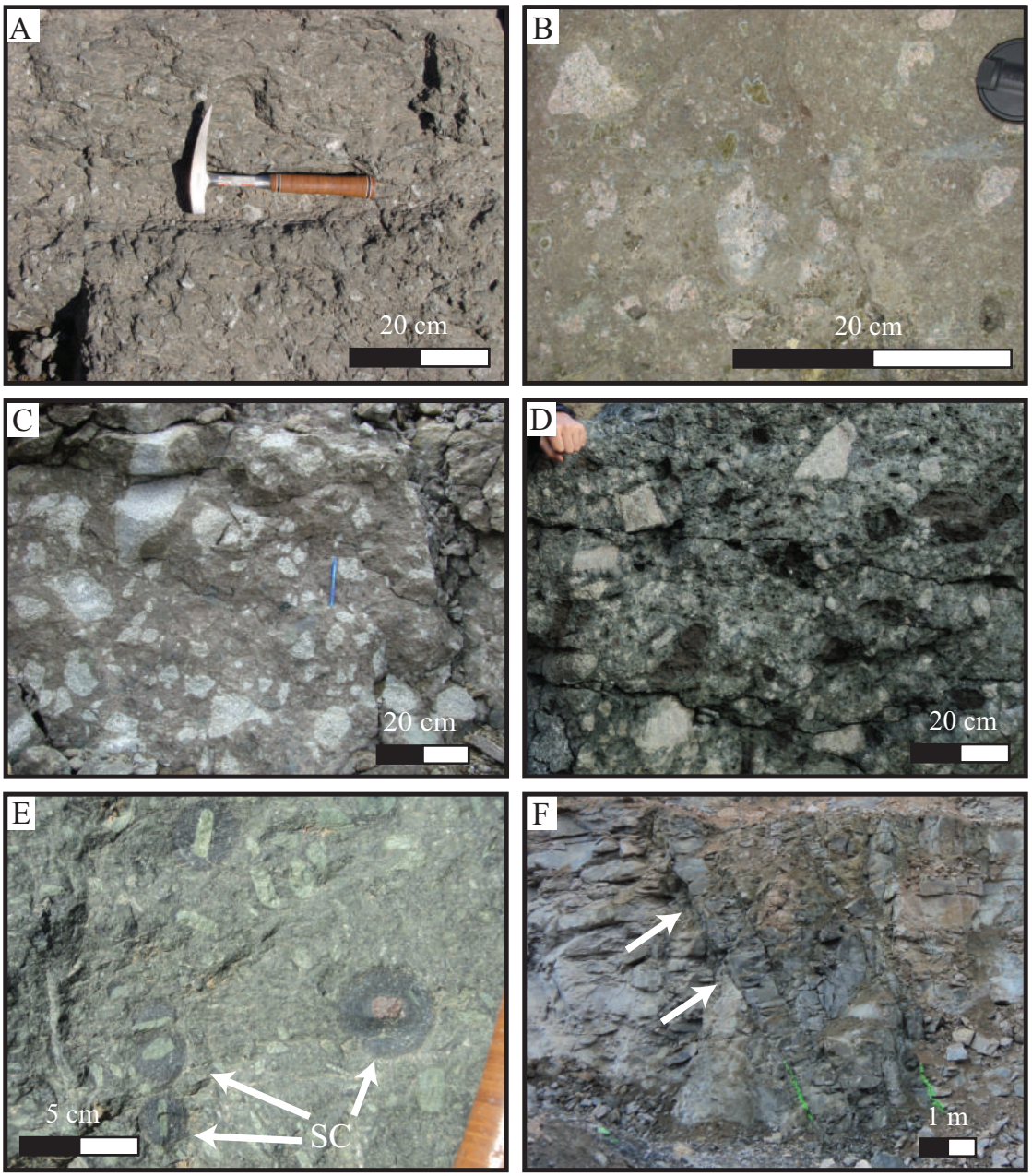

Fig. 5. Photographs of open-pit exposures of the main kimberlite rock types at K1: A) K1-KIMB1 (coherent kimberlite). B) K1-KIMB2 (volcaniclastic kimberlite). C) K1-KIMB3 (coherent/volcaniclastic kimberlite). D) K1-KIMB4 (volcaniclastic kimberlite). E) K1-KIMB5 (coherent kimberlite; note cored spherical clasts [SC]). F) K1-KDYKE (coherent kimberlite) indicated by white arrows. Rocks are described more fully in Table 1 and in Moss et al. (2013).

K3

K3 is a steep-sided, elongate, and L-shaped pipe occurring approximately 300 m north of K1 (Fig. 2). It is 100 m long in a north-south direction and a maximum of 75 m wide in an east-west direction at the northern one-third of the pipe. Minimal drilling data are available from K3, but current data indicate a complex internal geology consisting of three different kimberlite types (K3-KIMB1 to K3-KIMB3), all comprising volcaniclastic kimberlite, as well as multiple phlogopite-rich coherent kimberlite dikes of unknown orientation apparently crosscutting the pipe and surrounding country rocks. The surrounding country rocks around K3 are relatively competent on the west and north sides, though the extensive brecciation and alteration apparent in the country rocks around K1 and K2 is apparent in the area in between the two lobes of K3 (Fig. 2). Overall, the rock types and deposit geometry at K3 appear broadly similar to those at K1.

Metasomatism

A striking feature associated with the Murowa kimberlites is the extensive fenitization of wall rock surrounding the pipes

Table 2. Summary of Key Attributes of K1-MPZ Rock Types

	K1-MPZ1	K1-MPZ2a	K1-MPZ2b	K1-MPZ3a	K1-MPZ3b
Diagnostic features	In situ fracturing	Clast rotation; blue-green cement	Angular elongate shards of syenite/granite	Very fine grained; "rock flour"	Poorly sorted and coarse grained; "rock flour"
Textural classification	In situ fractured syenite	Granite breccia	Granite breccia	Tuffisite	Granite breccia in tuffisite
Dominant structure	In situ fracturing; discontinuous	Massive at 1- × 1-m scale	Massive at 2- × 2-m scale	Massive with local flow banding at 2- × 2-m scale	Clast rotated; massive at 5- × 5-m scale
Dominant framework	Thin interconnected veins	Clast and matrix supported	Clast and matrix supported	Matrix supported	Matrix supported
Degree of sorting	No sorting	Poorly sorted	Poorly to moderately sorted	Moderate to well sorted	Poorly sorted
Component distribution	In veins and small breccia pockets	Homogeneous	Heterogeneous	Homogeneous	Heterogeneous
Total olivine abundance (%)	0–2	0–5	0–2	0–10	0–6
Kimberlite clast abundance	0	0–1	0	0–2	0–2
Relative groundmass/ matrix size[1]	Coarse	Fine	Fine	Very fine	Very fine and very coarse
Groundmass/matrix minerals	Amph; cpx; carb; serp	Amph; cpx; carb; serp	Feld; qtz; amph; cpx; carb; serp	Feld; qtz; amph; cpx; carb; serp	Feld; qtz; cpx; carb; serp; amph
% CRX	85–99	80–95	60–98	40–85	50–75

Abbreviations are as follows: car = carbonate, cpx = clinopyroxene, CRX = country rock xenoliths, feld = feldspar, gnt = garnet, mont = monticellite, phl = phlogopite, pvk = perovskite, qtz = quartz, serp = serpentine

[1] Size classes based on Scott-Smith et al. (2013): uf = ultrafine, <0.125 mm; sf = superfine, 0.125–0.25 mm; vvf = very, very fine, >0.25–0.5 mm; vf = very fine, >0.5–1 mm; f = fine, >1–2 mm; m = medium, >2–4 mm; c = coarse, >4–8 mm; vc = very coarse, >8–16 mm; uc = ultracoarse, >16 mm

and dikes at both Murowa and the nearby Sese pipe cluster 70 km to the east (Fig. 1; Smith et al., 2004). The recognition of this fenitization was a major factor in the discovery of the Murowa kimberlites (Sims et al., 2018), and geologic modeling at Murowa has revealed the aureoles of fenitization form a "damage zone" which can be much greater than the surface area of the enclosed kimberlite pipe at a given depth (Moss et al., 2013). Damage zones as described here are a feature characteristic of some other kimberlite pipes (Harder et al., 2013; Muntener and Smith, 2013; Smith et al., 2013).

The fenitization comprised metasomatism that desilicified the granite country rock and converted it to syenite, with reddening of feldspars caused by hematite dusting and an overall green color reflecting chloritization. The change is apparently progressive, marked initially by spotting with chlorite and needles of alkali pyroxene and amphiboles and minor carbonate and talc development. Metasomatic veining appears more intense inward toward the kimberlite and leads on to brecciation of country rock and minor injection of kimberlite veins. At the main pipe contact and in isolated pockets in the marginal pipe zone around the pipes, slivers and plates of granite are apparent and assume a steep, inward-dipping orientation. Figure 9 displays the compositional contrast between the fenite and the various kimberlite types at Murowa, normalized to unaffected granite. The composition of the fenite is intermediate between unaffected granite and kimberlite (Fig. 9), suggesting a close association between the metasomatizing fluids and the kimberlite. The metasomatism is thus ascribed to fluids from the rising kimberlite melt penetrating into cracks and matrix of granite country rock and reacting with it. The fluids were apparently CO_2 rich, hydrous, oxidizing, enriched in ultramafic elements, and they carried low levels of Na (Fig. 9). These are characteristics broadly similar to fenitization observed around carbonatites and country-rock alteration adjacent to lamproites and other alkaline lamprophyre types (Smith et al., 2004).

Implications for kimberlite emplacement mechanisms

The textural features indicated among the rocks of K1 were previously interpreted to reflect a variety of emplacement processes. These processes include the following: (1) veining, fracturing, and metasomatizing of country rock (e.g., K1-MPZ1); (2) localized, gas-driven fluidization processes producing tuffisite-like (Cloos, 1941) fragment mixtures (e.g., K1-MPZ2a); (3) short-lived and pulsatory fracture and/or fragmentation driven by kimberlite dikes and associated kimberlitic fluids (e.g., K1-MPZ2b); (4) channelized and protracted fluid intrusion brecciation (e.g. K1-MPZ3a, 3b); and (5) explosive but incomplete magmatic fragmentation and mixing process between country-rock fragments and disrupting coherent kimberlite (e.g., K1-KIMB4; Moss et al., 2013). The textural features and processes interpreted to produce them are combined with apparent crosscutting relationships to indicate multiple emplacement events at K1 involving

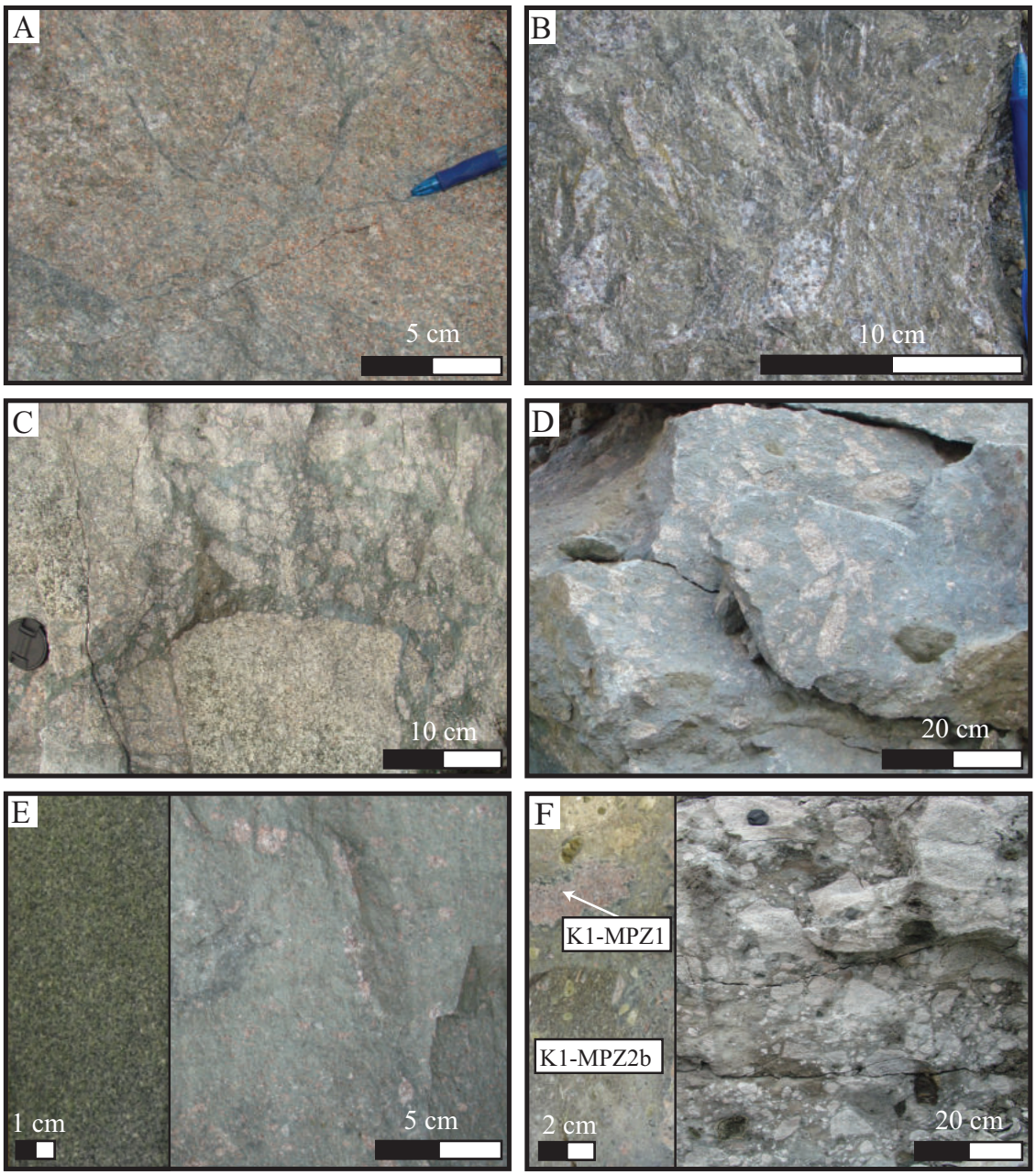

Fig. 6. Photographs of open-pit exposures of rock types from the marginal pipe zone of K1 (K1-MPZ): A) K1-MPZ1. B) K1-MPZ2a. C) K1-MPZ2b. D) K1-MPZ3a. E) K1-MPZ3b. A close-up of drill core showing rock-flour texture is shown on the left. Pipe-infilling K1-KIMB4 (volcaniclastic kimberlite) is shown again in F. F) A close-up of drill core showing K1-MPZ1 and K1-MPZ2b xenoliths in K1-KIMB4 is shown on the left.

kimberlite magmas with varying proportions of gas, liquid, and solid phases. Lithic fragments of K1-MPZ rock types are present within K1-KIMB2, K1-KIMB4, and K1-KIMB5, suggesting the country-rock brecciation and fragmentation by solid- and melt-poor kimberlite fluid was an early event relative to the emplacement of pipe-filling volcaniclastic kimberlite rocks at K1. These observations require interactions between temporally discrete ascending kimberlite magmas and different country-rock regimes with variable amounts of previously disrupted (fractures, brecciation) country-rock and ambient meteoric fluids, intruding/erupting over contrasting timescales (Moss et al., 2013).

A less explosive emplacement style is interpreted for K2 relative to K1 and K3, based on the textural features apparent in the main infill of the pipe. The lack of pyroclastic textures, lack of significant internal organization, even distribution and generally limited size of country-rock xenoliths (<20 cm), and overall homogeneous size distribution of olivine grains are interpreted to indicate relatively rapid, albeit passive, emplacement of kimberlite magma following extensive and

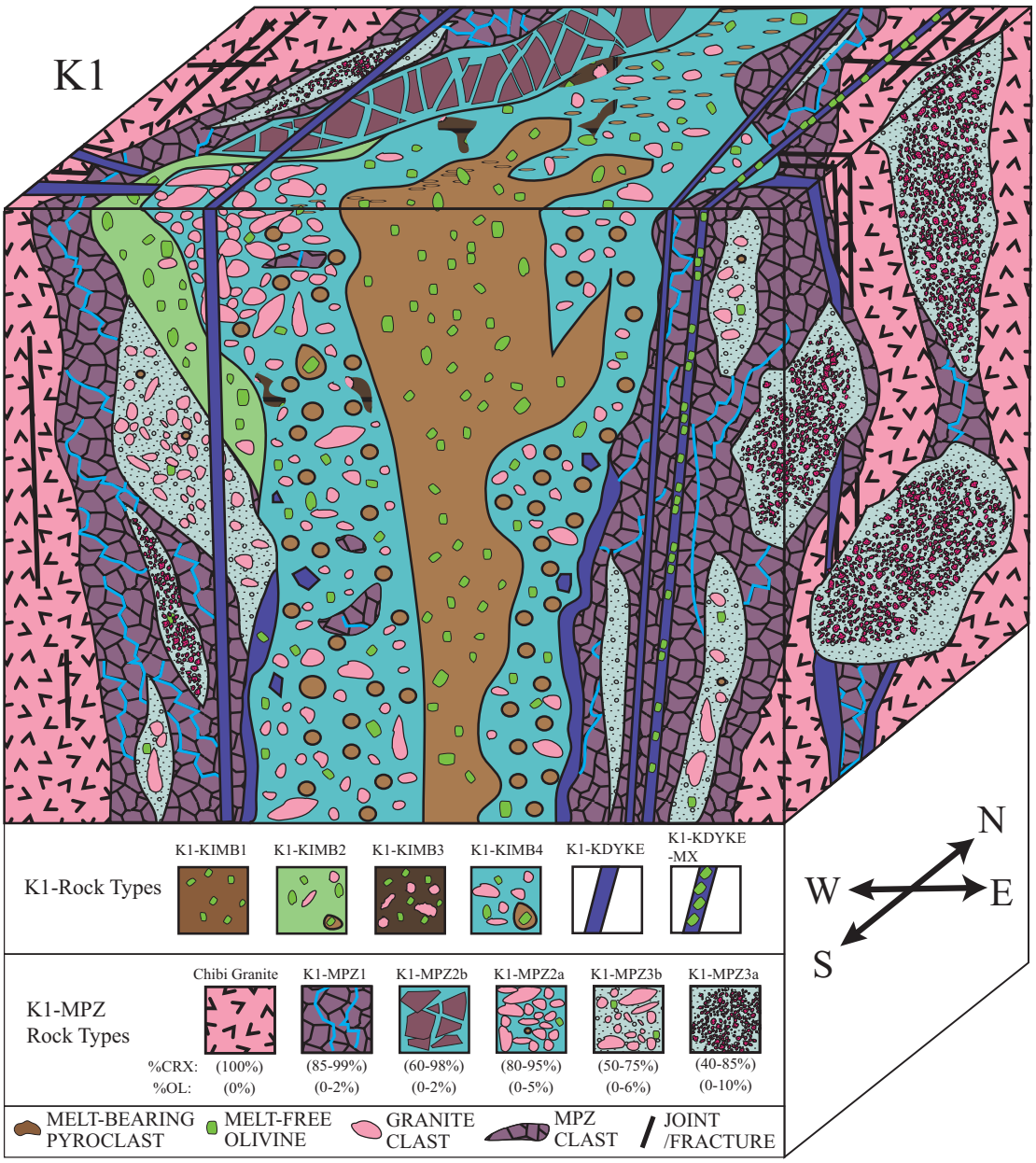

Fig. 7. Schematic figure illustrating the distribution and contact relationships between main kimberlite rock types and marginal pipe zone rock types in K1: K1-KIMB1 (coherent kimberlite); K1-KIMB2 (volcaniclastic kimberlite); K1-KIMB3 (coherent/volcaniclastic kimberlite); K1-KIMB4 (volcaniclastic kimberlite); K1-KIMB5 (coherent kimberlite); K1-KDYKE (coherent kimberlite); K1-KDYKE-MX (coherent kimberlite); K1-MPZ rock types (variable granite breccias ± kimberlite components).

potentially highly explosive excavation of variably brecciated and altered granite and mylonite.

Geologic Models

The observations described above and the spatial distribution of logging and mapping data allow 3-D geologic models to be produced for K1, K2, and K3. Each geologic domain modeled in three dimensions comprises one or more of the major rock types described above, all of which have been identified in multiple drill cores and/or open-pit exposures and confirmed by petrography (Moss et al., 2013). Six geologic domains have been modeled at K1: K1-KIMB1, K1-KIMB2, K1-KIMB4, K1-KIMB5, K1-KDYKE-MX, and K1-MPZ (Fig. 10A-C). K1-KIMB3 has been included within the K1-KIMB4 domain. At K2, K2-KIMB1 and the K2-MPZ have been modeled in three dimensions. K2-KIMB1 at K2 is separated into two domains: the K2-MAIN pipe and the K2-West bulge (Fig. 10D-F). The latter is characterized by a significantly higher frequency of K2-KDYKE-INT intersections. K2-KIMB2 is interpreted to be a volumetrically minor pipe infill, and the thin intersections of this rock type have been modeled within K2-KIMB1. At K3, a simple pipe shell

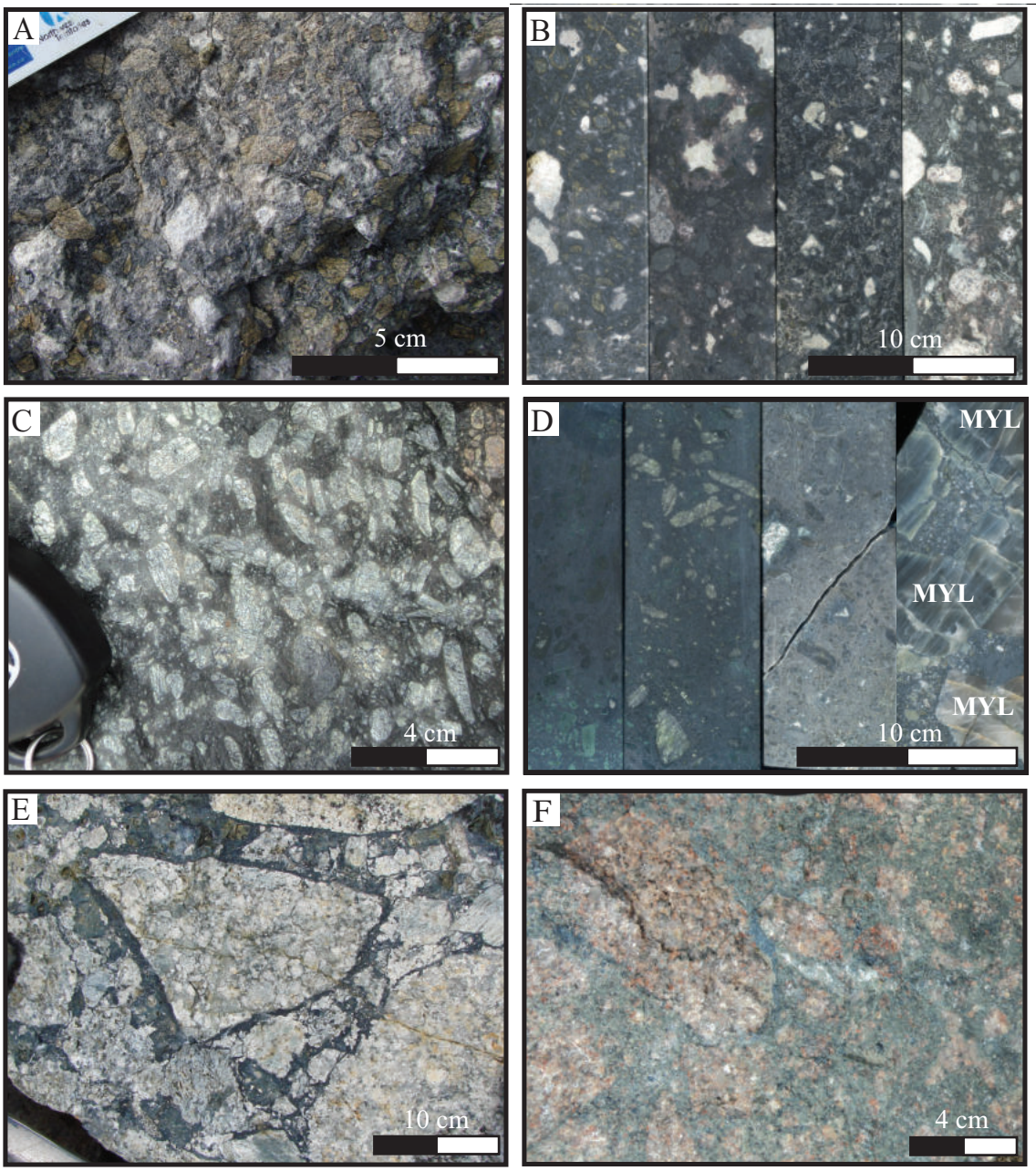

Fig. 8. Photographs of open-pit exposures and polished slabs of the main rock types at K2: A) Open-pit exposure of K2-KIMB1 (coherent kimberlite). B) Polished slabs of K2-KIMB1. C) Open-pit exposures of KDYKE-INT (coherent kimberlite). D) Polished slabs of KDYKE-INT. Note KDYKE-INT intruding and brecciating mylonite (MYL) from the Quartz Shear at far right of image. E, F) Examples of K2-MPZ (variable granite breccias ± kimberlite components).

has been modeled to include all rock types (K3-MAIN; Fig. 10G, H) on the basis of drill hole intercepts, and no internal geology has been developed.

Structural Geology

Methods

Rio Tinto Exploration (RTX) investigated the structural geology of the region around Murowa during the late 1990s with the primary goal of understanding the structural controls on kimberlite emplacement. This investigation allowed RTX to rank targets and/or find additional resources in the immediate area of the project and define the overall structural setting of the project. To this end, field studies were conducted comprising photogeologic mapping and interpretation using 1:25,000 air photos and photo enlargements of a 14- × 20-km area, examination of drill cores, regional magnetics, and aeromagnetic imagery (Marten, 1999a, b). The key results and interpretations from this study are summarized below.

Table 3. Summary of Key Attributes of K2 Kimberlite Rock Types

	K1-MAIN	K1-WestBulge	K2-KIMB2	K2-KDYKE type A
Diagnostic features	Altered white crx; coarse conspicuous olv; finer felted phl groundmass	Altered white crx	Altered white crx + shards; ± less coarse olv; phl phenocrysts; coarser sp	Rare crx; coarse conspicuous olv; phl ≈ mont %; poikilitic phl
Textural classification	Coherent kimberlite	Coherent kimberlite	Coherent kimberlite	Hypabyssal kimberlite
Mineralogical classification	Monticellite phlogopite	Monticellite phlogopite	Monticellite phlogopite	Monticellite phlogopite
Hardness	Hard	Hard	Hard	Very hard
Color	Dark brown to black	Dark brown to black	Dark brown to black	Dark gray to black
Dominant structure	Massive ± flow aligned	Massive ± flow aligned	Massive	Massive/flow aligned
Dominant framework	Groundmass supported	Groundmass supported	Groundmass supported	Groundmass supported
Degree of sorting	Poorly sorted	Poorly sorted	Poorly sorted	Poorly sorted
Component distribution	Homogeneous	Homogeneous	Homogeneous	Homogeneous
Total olivine abundance (%)	45–50%	45–50%	45–50%	45–50%
Olivine size range[1]	Very fine to very coarse	Very fine to very coarse	Very fine to very coarse	Very fine to very coarse
Olivine > 1 mm (%)	20–25%	20–25%	20–25%	20–25%
Kimberlite clast abundance	Rare "pseudoclasts"	Absent	Absent	Absent
Country-rock xenolith abundance	5–35%	5–30%	5–20%	0–5%
Dominant xenolith types	Granitoid/mylonite	Granitoid	Granitoid	Granitoid
Relative groundmass/matrix size[1]	Fine	Fine	Coarse	Coarse
Groundmass minerals	Phl, mont, sp, pvk	Phl, mont, sp, pvk	Phl, mont, sp, pvk	Phl, mont, sp, pvk ± apt
Mantle xenoliths and xenocrysts	Peridotite microxenoliths; Gnt and sp	Peridotite microxenoliths; Gnt and sp	Rare to absent	Rare to absent

Abbreviations are as follows: car = carbonate, cpx = clinopyroxene, crx = country-rock xenoliths, gnt = garnet, harz = harzburgite, ilm = ilmenite, lherz = lherzolite, mont = monticellite, olv = olivine, phl = phlogopite, pvk = perovskite, serp = serpentine, sp = spinel

[1] Size classes based on Scott-Smith et al. (2013): uf = ultrafine, <0.125 mm; sf = superfine, 0.125–0.25 mm; vvf = very, very fine, >0.25–0.5 mm; vf = very fine, >0.5–1 mm; f = fine, >1–2 mm; m = medium, >2–4 mm; c = coarse, >4–8 mm; vc = very coarse, >8–16 mm; uc = ultracoarse, >16 mm

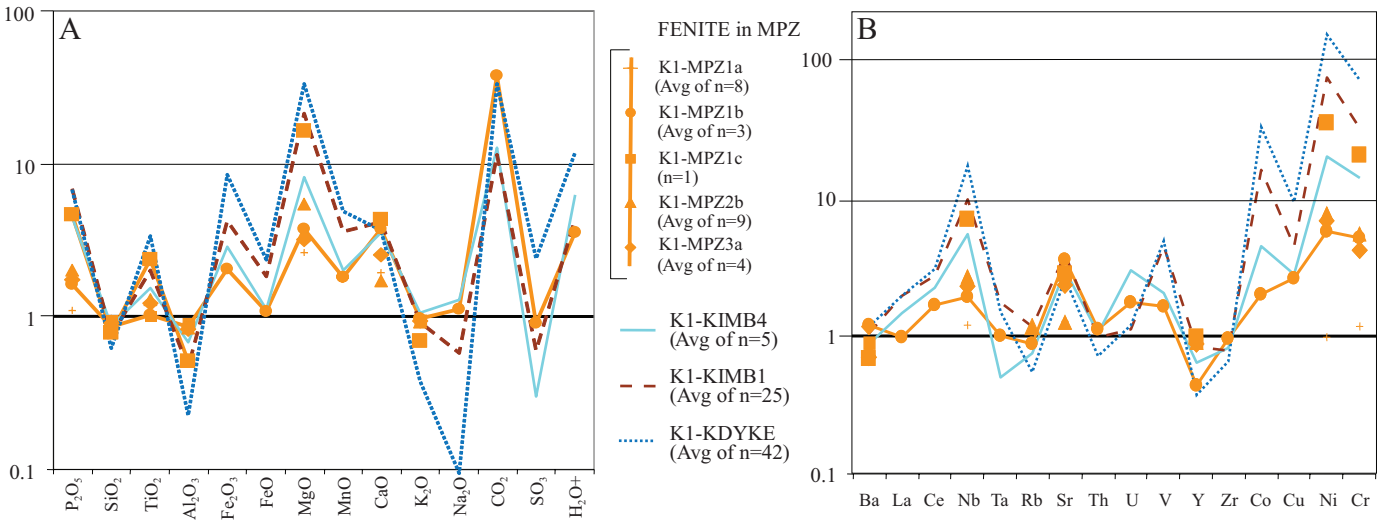

Fig. 9. Murowa kimberlite and fenite major and trace element chemistry normalized to Chibi granite = 1: A) Major element chemistry shown for main kimberlite rock types in K1 and a selection of K1-MPZ rock types representing metasomatized granite (syenite) or fenite described by Smith et al. (2004). B) Trace element chemistry shown for the same rock types. The composition of the fenite is intermediate between unaffected granite and kimberlite.

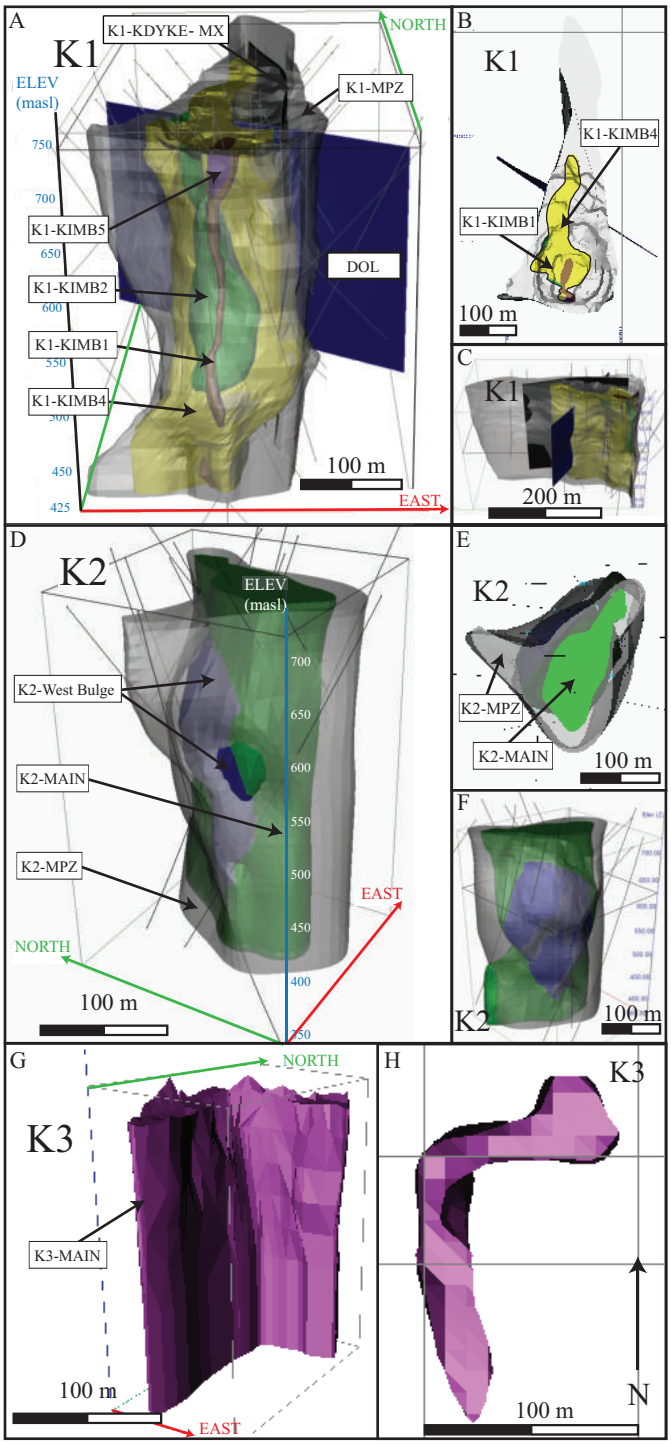

Fig. 10. 3-D geologic models for K1, K2, and K3 at Murowa: A) Inclined view from above facing north, plan view (B), and profile view (C) facing east of K1 geologic model comprising K1-KIMB1 (brown), K1-KIMB2 (green), K1-KIMB4 (yellow), K1-KIMB5 (purple), K1-MPZ (transparent gray), K1-KDYKE-MX (black), and a marker dolerite dike, DOL (dark blue). D) Inclined view from above, facing northeast, plan view (E) and profile (F) of K2 geologic model comprising K2-MAIN (green), K2-WestBulge (blue), and K2-MPZ (transparent gray) domains. (G) Inclined view from above facing northwest of K3 geologic model comprising K3-MAIN. (H) Plan view showing K3 geologic model.

Results

Kimberlite clusters in the region as a whole appear to show an east-west alignment, as the Murowa pipes combined with nearby kimberlite clusters trend at approximately 093° (Marten, 1999a), while the pipes within the Murowa cluster show an approximately north-south trend (Fig. 2). The Chibi batholith hosting the Murowa kimberlite has no evidence of any homogeneous tectonic strain but contains minor brittle fracturing, and the apparent bulk strain is negligible. Joint development is of variable intensity, and air photo lineaments reflect zones of more intense fracturing. The granite is, in many places, massive and poorly jointed, resulting in kopje development through weathering and exfoliation processes. The granite is cut by two main sets of shear fractures and joints: an NNE-trending set, termed the Quartz Shear set, and an NW-trending set (Marten, 1999a, b). The two sets have different characteristics and therefore do not form a conjugate system. The path of the nearby Lundi River closely follows a major NW-trending lineament that appears to be offset by the Quartz Shear (Fig. 11), which would thus appear to be the younger of the two. The Lundi River lineament may be unrelated to the main NW-trending fracture system (which postdates the Quartz Shear; see below) because it has an unusually strong magnetic signature.

The NNE set: This structural set, comprising closely spaced joints and fractures, was first described by Robertson (1974), who noted characteristic lenses of quartz. The most prominent feature of this set in the Murowa area is the "Quartz Shear," a 15- to 50-m-wide composite zone comprising bands of laminated siliceous mylonite (10 cm–1 m thick), in foliated to protomylonitic granite containing diffuse sheared quartz veins merging into lenses of mylonite. The Quartz Shear is well exposed in the Lundi River and forms a positive linear topographic feature due to zones of pervasive silicification. The Quartz Shear passes on the east side of the Murowa kimberlite group on an orientation of 020°. Joints on this orientation are observed throughout the Murowa area to the west of Quartz Shear, and fractures observed in the field are tight and usually healed with silica (Marten, 1999a). This appears to be reflected in a relatively weak aeromagnetic and resistivity expression compared to the NW-trending set. The shear contains a stretching lineation that plunges 35° to 65° to the north-northeast, and vertical surfaces show well-defined shear bands that indicate the southeast side has moved down and the northwest side has moved up. Sinistral shear is observed on some horizontal surfaces in this zone (Fig. 12), as well as sinistral shear shown by left-stepping dilational offsets, or "tensile bridges" (sensu Gamond, 1987). An ovoid zone of quartz vein stockwork measuring 45 × 15 m is exposed at the south end of the open pit at K2, with the long axis parallel to the 020° shear fractures (Fig. 12). Parallel shears are apparent to the northwest, the closest of which passes just west of K3, where it is expressed as an aeromagnetic lineament.

The NW set: The NW-trending photolinears are the expression of 10- to 20-m-wide zones of relatively closely spaced (0.25–1.5 m), NW-trending subvertical joints (Figs. 11, 12). The northwest set has a stronger topographic and geophysical expression than the north-northeast set, appearing to be a more strongly developed system in part because of the lack

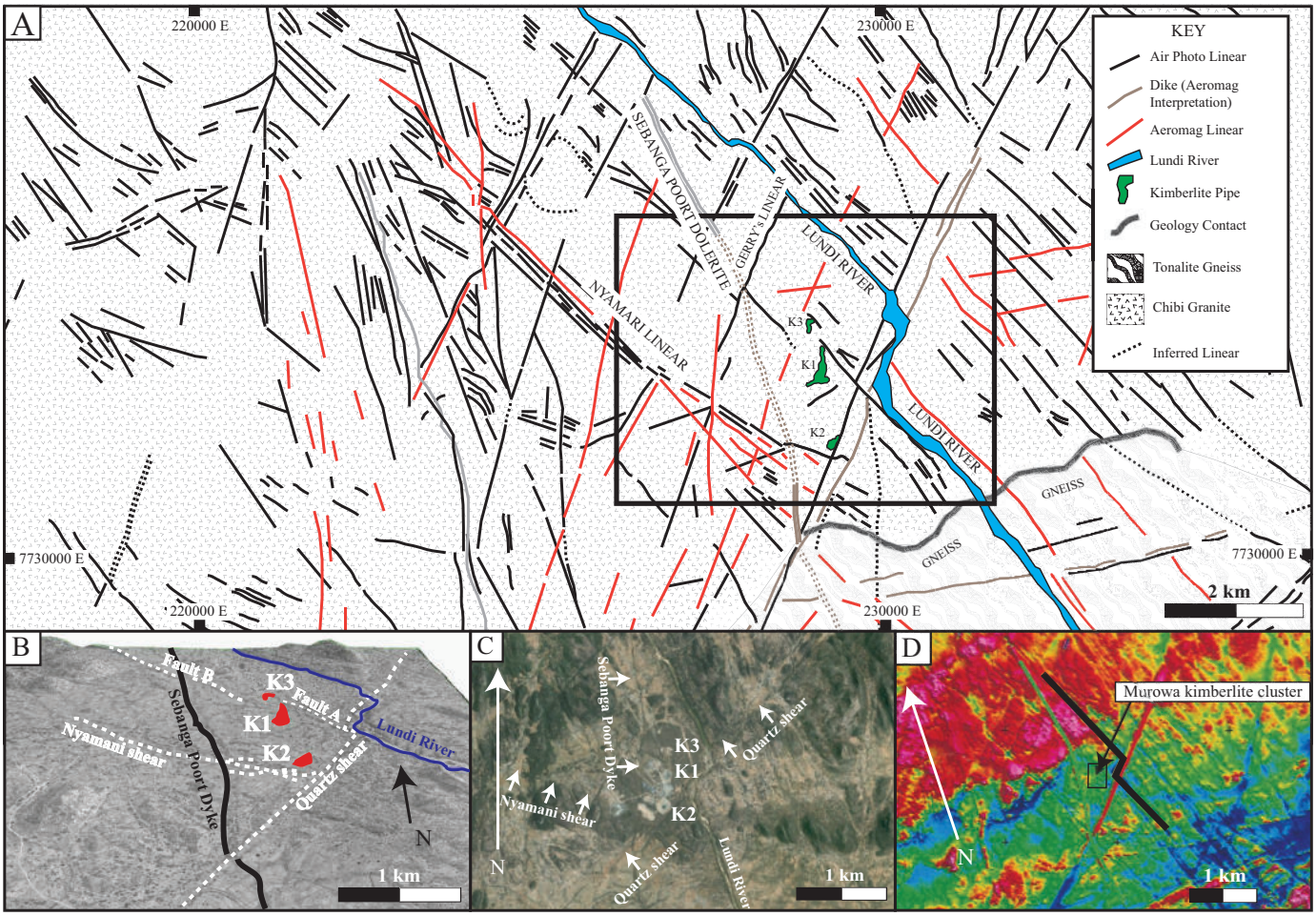

Fig. 11. Structural mapping in Murowa area: A) Structural map showing interpreted linears from air photos, aeromagnetic data, and approximate locations of kimberlite, Chibi granite, and tonalite gneiss at 1:25,000 scale. Black box shows approximate location for (B) and (C). B) Inclined air photo of Murowa area facing approximately north, showing interpreted linears (white dashed lines) and a splay of the Sebanga Poort Dyke (black line). C) Plan-view air photo showing kimberlite pipes K1, K2, and K3 at Murowa diamond mine and interpreted structural features. Image courtesy of GoogleEarth™. D) Aeromagnetic data supporting air photo interpretation. Black line indicates approximate location of Lundi River.

of healing or sealing of the fractures by silicification. Three of the most prominent linears were traversed: two in the K1-K3 area, labeled "A" and "B" (Fig. 11B), and the Nyamari lineament that strikes south of K2. Linear A strikes at 315° from the Lundi River across the end of K1 before attenuating, with shearing evident in the displacement of the Quartz Shear by approximately 50 m in a sinistral sense. A kimberlite dike apparent in the Lundi River bed occupies this structure and shows locally sheared contacts (Marten, 1999a). Linear B is a zone similar to linear A of close-spaced jointing, with only minor evidence for shearing in the form of a 1-cm left-lateral displacement of a pegmatite across one joint. The Nyamari linear is broadly similar to linears A and B but consists of a wider zone of jointing expressed as closely spaced photolinears in the northwest, which weakens and deflects to a more east-southeast trend toward K2, where it attenuates. The interpretation of aeromagnetic data and air photos suggests a splaying out of the structure in this area, against a lineament occupied by the Sebanga Poort Dyke (Fig. 11). Shear fractures and a zone of crushing are apparent throughout the Nyamari linear, indicating that the linear represents a fault similar to linear A.

Interpretation

The structural data sets allow for two interpretations that identify potential structural mechanisms for the emplacement of kimberlite in the Murowa area (Fig. 13). Firstly, the Quartz Shear and a parallel shear just west of K3 are interpreted to be related structures leading to the development of a sinistral tensile bridge in the area between them. The dilation fractures in this system would be approximately north-south. Secondly, linears A and B are interpreted as related en-echelon sinistral shears, and the gap between the two can also be interpreted as a tensile bridge, which would have been subject to dilational fracturing in an approximately east-west orientation, in contrast with those developed by the north-northeast set. The sense of fanning of the Nyamari linear into a splay suggests that it may be the edge of a large-scale tensile bridge structure in a sinistral shear system and would thus extend the domain of tensile fracturing predicted in the bridge between linears A and B.

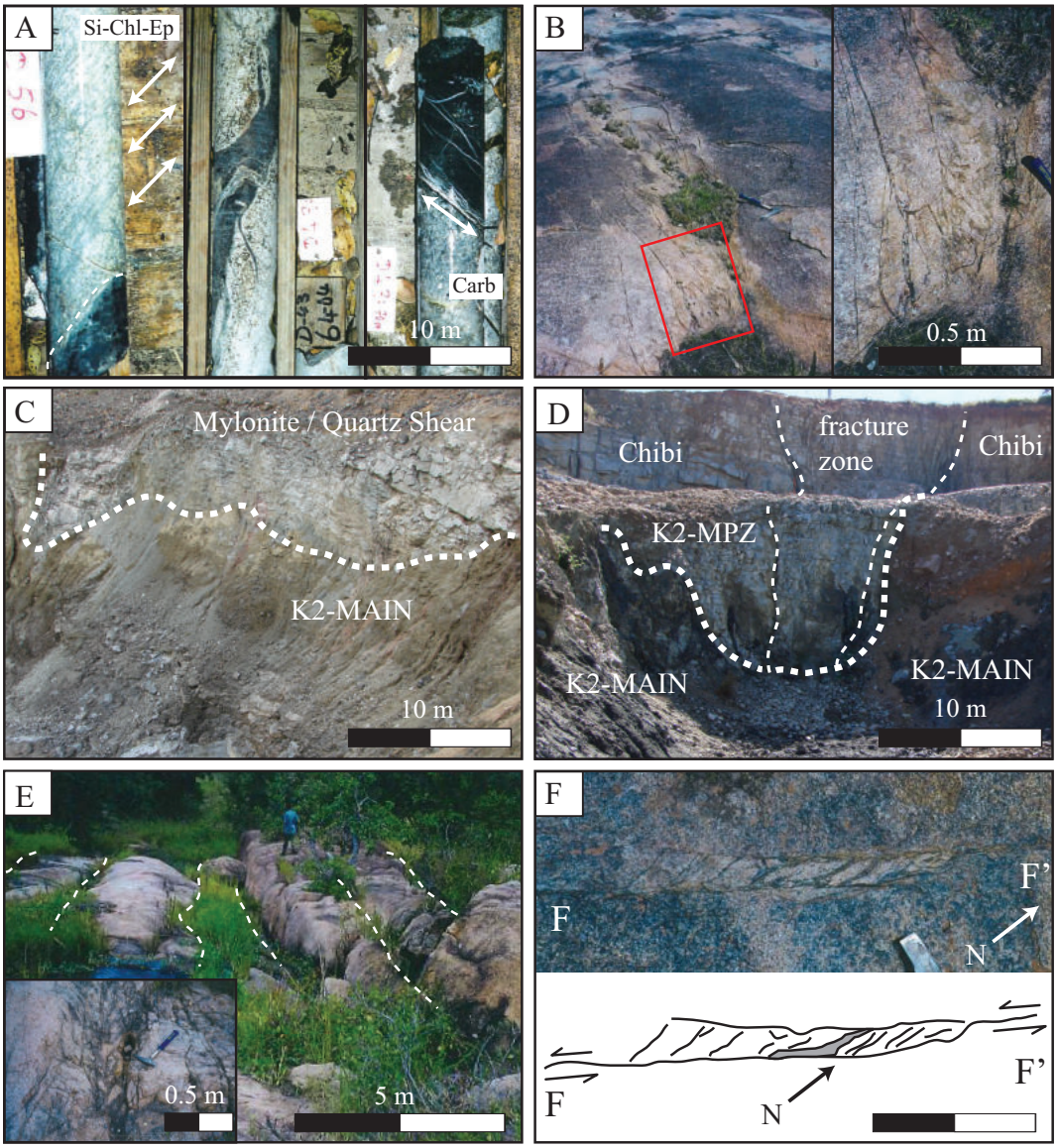

Fig. 12. Photographs of structural features from drill core and mapping in the Murowa area: A) Drill core from country rock around K2: left panel—sharp planar contact of KDYKE with granite, parallel to green shears of the NNE set (020°; parallel to white arrows), which are mineralized by silica-chlorite-epidote (Si-Chl-Ep); middle panel—sigmoidal tension gash veins peripheral to a KDYKE, showing a left-lateral shear sense in this view; right panel—example of a sheared planar dike contact mineralized by carbonate (Carb). B) Example of a sinistral tensile bridge structure in an NNE set shear fracture (020°). Inset: Close-up of (B) showing local breccia with granite shards similar to those in K1-MPZ2b. C) View facing southeast of open pit at K2 showing contact between K2-MAIN and mylonite country rock and the Quartz Shear structure. D) View facing north showing northern margin of K2-MAIN in contact with K2-MPZ and fresh Chibi granite, and zone of closely spaced joints and fractures striking north, extending approximately 30 m horizontally from the pipe margin (foreground) to the high wall of the open pit (background). Contacts are shown by white dashed lines. E) View facing east-southeast along the strike of the Nyamari linear showing closely spaced joints (white dashed lines). Inset: Close-up of Nyamari linear showing a fracture and crush zone with incipient brecciation, striking southeast approximately 800 m west of K2. F) Dilational step or "tensile bridge" in a shear fracture that shows a sinistral sense of movement, from an outcrop 900 m west of Nyamari stream. The veins are filled with silica-chlorite-epidote–altered rock flour or microbreccia. Note that the linking microbreccia veins have a northerly strike. The interpretation of F to F" is shown below, with black arrows indicating the shear sense.

These interpretations have contrasting implications for the development of tensile cracking but are not considered to be mutually contradictory, as the physical memory of tectonic events can be long retained as features within cratonic rocks. Moreover, the primary features and different tensile cracking orientations resulting from both interpretations are further supported by the geometry, componentry, and spatial distribution of the kimberlite pipes and dikes in the Murowa area. The K1, K2, and K3 kimberlites are aligned north-south, and the multilobed K1 and K3 are both dominantly elongate in a north-south direction, as are numerous kimberlite dikes found crosscutting K1 and K2, and the thick

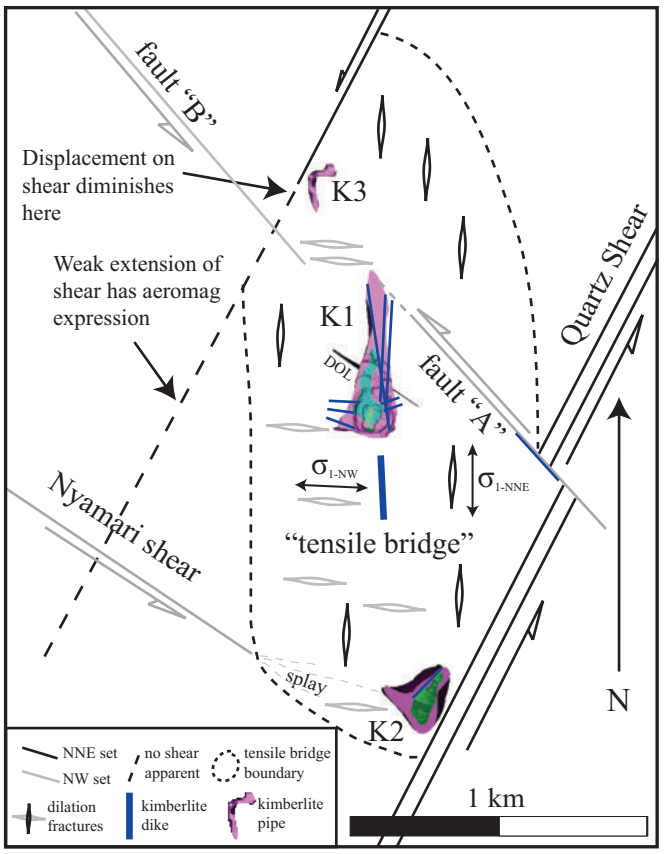

Fig. 13. Structural model of Murowa area. Two sets of structural features (NNE set, NW set) associated with different ages are interpreted to generate superimposed tension cracks in north-south and east-west directions, which controlled the spatial distribution, orientation, and geometry of emplaced kimberlite. The symbols $\sigma_{1\text{-NNE}}$ and $\sigma_{1\text{-NW}}$ signify the orientations of highest compressive stress which would derive from shear, as indicated in the figure for the NNE and NW sets, respectively. See text for details.

kimberlite dike observed just south of K1. Importantly, the N-S–oriented planar kimberlite dikes are parallel to and within the set of fractures, occupied by seams or veinlets of silica-chlorite-epidote, and the dike contacts are sheared and slickened (Fig. 12). Conversely, several kimberlite dikes observed on the west side of the K1 pit crosscut the K1-MPZ in an approximately east-west orientation (Figs. 2–4). The K1 and K3 pipes also have prominent lobes extending in an east-west orientation. A kimberlite dike infills a part of linear A, and K2 is elongate in a northeast-southwest direction at approximately 020° and is adjacent to the Quartz Shear (Fig. 2), suggesting kimberlite was also emplaced into both of the structural sets.

Radiometric Dating of K1 and K2

To constrain the emplacement ages of the Murowa kimberlites, samples of coherent kimberlite (KDYKE) spatially associated with K1 and K2 were analyzed using three independent radiogenic isotope techniques: Rb-Sr dating of phlogopite, U-Pb dating of perovskite, and $^{40}Ar/^{39}Ar$ dating of phlogopite. Two KDYKE-EXT samples (K1-D104; K1-D027) were collected from drill core near the contact with K1-KIMB4 and are interpreted to be from the deeper extension of an NNE-striking kimberlite dike readily observable in the K1 open pit. The dike crosscuts marginal pipe zone rock types but is apparently crosscut by K1-KIMB4, suggesting it was emplaced prior to the main pipe-forming event at K1. One KDYKE-INT sample from K2 (K2-D083) was collected from drill core within K2-MAIN and is interpreted to be from the deeper extension of a 020°-striking kimberlite dike that is apparently contained within the K2 pipe margins. The dike clearly crosscuts K2-MAIN in both drill core and the K2 open pit, and was thus emplaced after the main pipe-forming event at K2. The key results are shown in Tables 4 and 5 and summarized below. Analytical methods are detailed in the digital appendix (Appendix 1).

Table 4. Rb-Sr Phlogopite Results

Sample no.	Rb (ppm)	Sr (ppm)	$^{87}Rb/^{86}Sr$	Error (%)	$^{87}Sr/^{86}Sr$	Error (%)	Age (Ma)	2σ
K2 D083	57	62	2.48	0.50	0.72288	0.01000	543.6	5.1
K1 D104	389	78	11.41	0.50	0.79546	0.01000	564.4	2.9
K1 D027	351	203	4.53	0.50	0.73776	0.01000	528.6	3.5
K1 D104 perovskite	0	>5,000	0.00	Not applicable	0.70363	0.01850	Not applicable	Not applicable

Table 5. Comparative Age Dates (Ma) from Different Methods for K1 D104, K1 D027, and K2 D083

Associated pipe	Sample no.	Rock	U-Pb	Rb-Sr	Ar-Ar
K1	K1 D104	KDYKE-EXT	513 ± 12	564.4 ± 2.9[1]	526.9 ± 1.2 526.5 ± 2.0
	K1 D027	KDYKE-EXT	Not applicable	528.6 ± 3.5	528.5 ± 2.2 525.7 ± 2.3
K2	K2 D083	KDYKE-INT	Not applicable	543.6 ± 5.1	Not applicable

[1] The Ar-Ar spectra for sample K1 D104 (see Digital Appendix) indicate phlogopite underwent slight alteration (see text), which would have perturbed the Rb-Sr system and rendered the Rb-Sr age determination unreliable in this case

Analytical results

U-Pb perovskite: Over two analytical sessions, 21 perovskite grains were analyzed from sample K1 D104. $^{207}Pb/^{206}Pb$ ratios ranged between 0.145 and 0.337, meaning the majority of Pb measured is radiogenic in nature and, thus, the age determination is less reliant on a well-constrained common Pb value. Using the Stacey-Kramers defined common Pb value of 0.870 ± 0.005, the perovskite defines an age of 512 ± 13 Ma (2σ error) with an MSWD of 9.4 when data are plotted on a Tera-Wasserburg plot (Fig. 14).

Rb-Sr phlogopite: Rb-Sr isotope data for phlogopite separates collected from K1 D104, K1 D027, and K2 D083 are shown in Table 4. A two-point isochron age was calculated for K1 D104, while model ages were calculated for samples K1 027 and K2 D083 using the initial Sr ratio determined for perovskite from sample K1 D104. A total of 18 perovskite grains were analyzed, resulting in the determination of an initial Sr value of 0.70363 ± 0.00013 (MSWD 0.99; Fig. 15A), which, combined with the apparent mineralogy in K1, suggests this body is consistent with other "group 1" kimberlites (Mitchell, 1995) and distinct from "group 2" kimberlites or "orangeites" (Smith, 1983). The three samples yield isochron or model ages of 564.4 ± 2.9 Ma (2σ; K1 D104), 528.6 ± 3.5 Ma (2σ; K1 D027), and 543.6 ± 5.1 Ma (2σ; K2 D083). Note that stated uncertainties for sample K1 D027 and K2 D083 reflect analytical precision only.

$^{40}Ar/^{39}Ar$ phlogopite: Detailed laser step-heating experiments were conducted on two phlogopite grains apiece from K1 D104 and K1 D027. Analytical results are summarized below and reported in full in the digital appendix (Table A1). Step-heating spectra (Fig. 16) were generated using ISOPLOT/Ex v.3.75 (Ludwig, 2012).

1. K1 D104: The two grains analyzed from sample K1 D104 yielded moderately discordant age spectra and did not produce statistically resolvable plateau ages (Fig. 16A). The

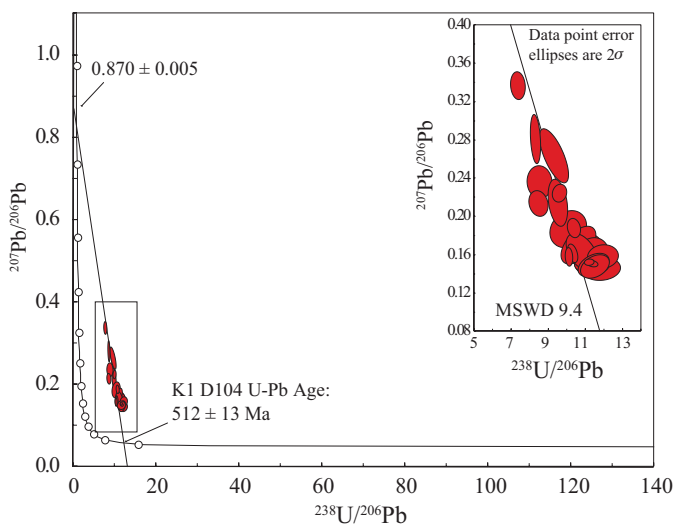

Fig. 14. Tera-Wasserburg plot of U-Pb in perovskite from sample K1-D104. Data from 21 perovskites were anchored to an appropriate Stacey-Kramers common Pb value (0.87 ± 0.005) in order to constrain a U-Pb in perovskite model age of 512 ± 13 Ma with an MSWD of 9.4. Data point error ellipses are 2σ. Expanded view of data is shown in inset.

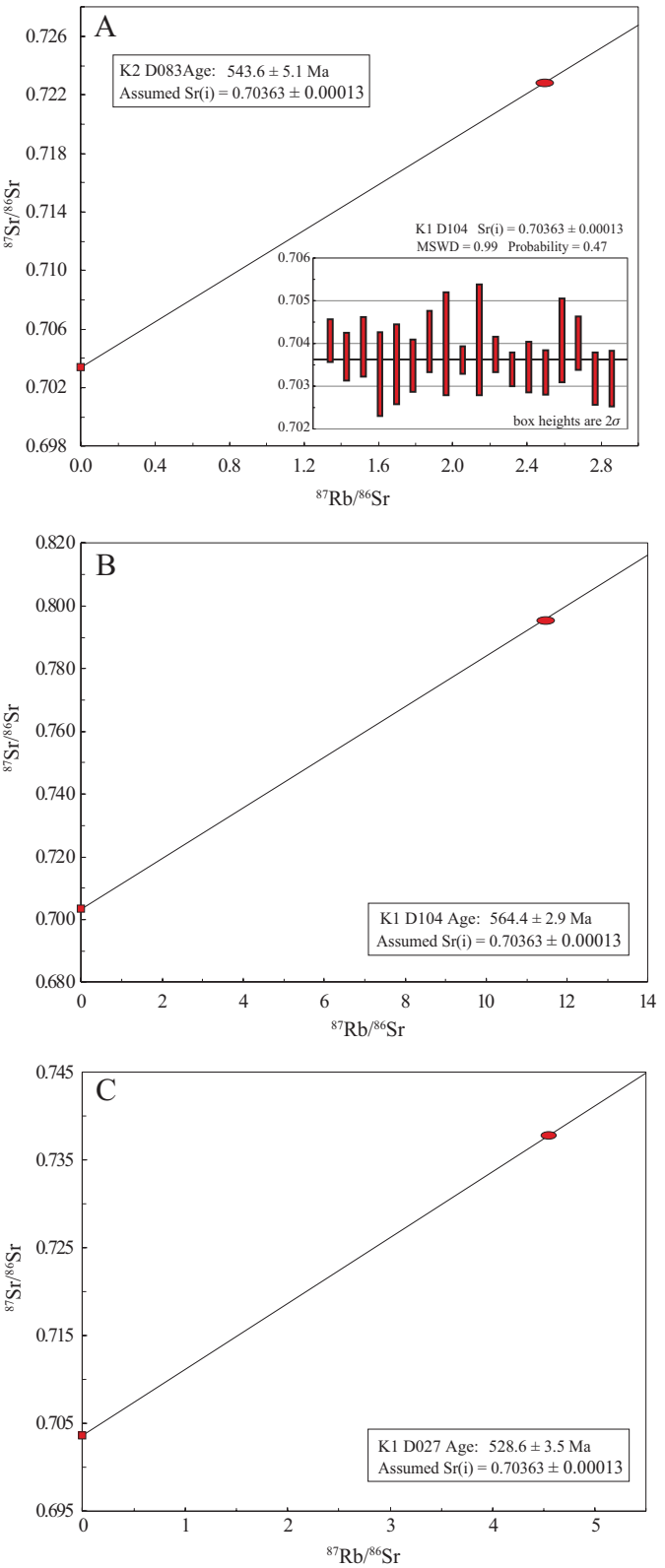

Fig. 15. Two-point isochron model ages on plots of the ratio of $^{87}Sr/^{86}Sr$ to $^{87}Rb/^{86}Sr$ from K1 and K2 samples: A) K2-D083: 543.6 ± 5.1 Ma. B) K1-D104: 564.4 ± 2.9 Ma. C) K1-D027: 28.6 ± 3.5 Ma. Model ages were calculated in all cases using the initial Sr ratio determined from 18 perovskite grains analyzed in sample K1-D104 (inset 14A: 0.70363 ± 0.00013; MSWD 0.99). Data point error ellipses (red) are 2σ.

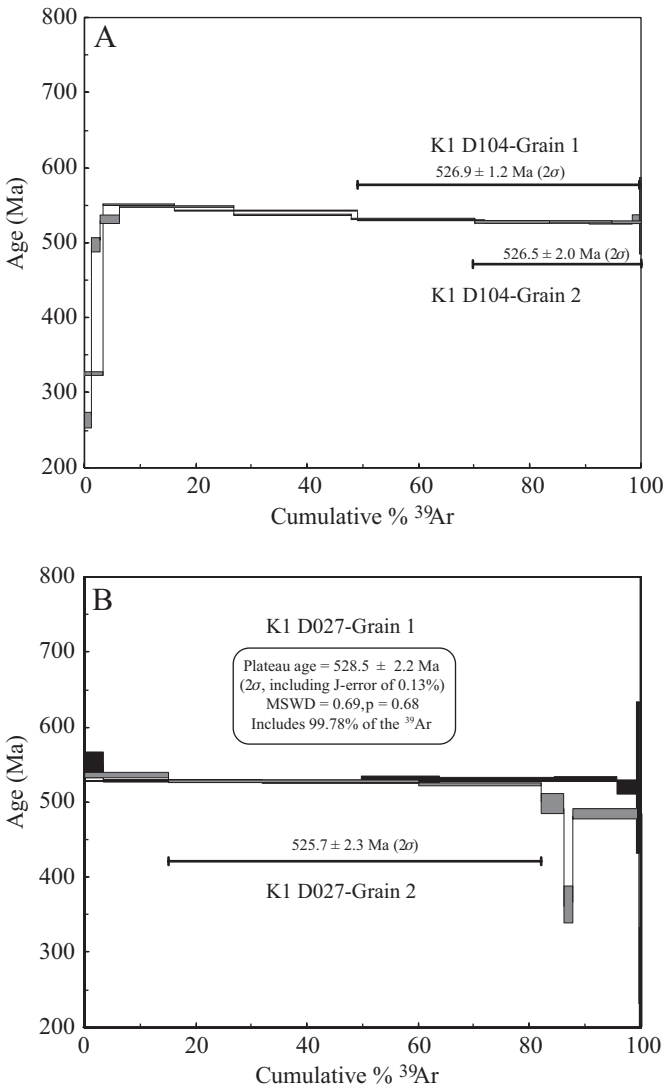

Fig. 16. Plots of cumulative % ^{39}Ar from step-heating experiments conducted on two phlogopite grains from samples of KDYKE crosscutting the main infill from K1 (K1-D104 and K1-D027): A) Concordant weighted mean ages for phlogopite grains from sample K1-D104 of 526.9 ± 1.2 (grain 1) and 526.5 ± 2.0 Ma (grain 2). B) Concordant plateau and weighted mean ages for sample K1-D027 grains 1 and 2, respectively. Plateau steps are black; rejected steps are gray. Box heights are 1σ. Parentheses indicate steps used to calculate weighted mean averages. Plots were generated using ISOPLOT/Ex v.3.75 (Ludwig, 2012).

young apparent ages calculated for the low-T heating steps may reflect partial ^{40}Ar loss from poorly retentive sites due to alteration. The decrease in apparent age (from ~550 to 526 Ma) with increasing temperature for the intermediate steps is also likely related to minor alteration of the phlogopite and recoil loss/redistribution of $^{39}Ar_K$ (e.g., Phillips et al., 1999; Jourdan et al., 2007; Hall, 2013). Age concordance improves for the higher-temperature steps in both experiments (Fig. 16A) and, therefore, weighted mean ages were calculated from these steps. This approach yielded highly concordant ages of 526.9 ± 1.2 Ma (steps 4–7, 51% of $^{39}Ar_T$) and 526.5 ± 2.0 (steps 7–9, 30% of $^{39}Ar_T$) for grain 1 (M7-1) and grain 2 (M7-2) at 2σ confidence, respectively.

2. K1 D027: The step-heating results for grain 1 (M8-1) produced a well-defined age plateau age of 528.5 ± 2.2 Ma (2σ; MSWD = 0.69, p = 0.68), incorporating data from eight of the nine heating steps ($^{39}Ar_T$ = 99.78%; Fig 16B). In contrast, the step-heating analyses for grain 2 (M8-2) did not produce a statistically resolvable plateau, with apparent ages decreasing with increasing temperature, suggesting significant recoil loss/redistribution issues in this grain. However, it is noted that only 16% of the total ^{39}Ar was released during the final three heating steps and that the ^{36}Ar signal measured for these steps was indistinguishable from background, such that apparent ages calculated for these steps are not particularly meaningful. Gas released from heating steps 2 and 3 comprises 67% of the total ^{39}Ar (Fig. 16B) and yields concordant apparent ages of 526.5 ± 2.3 Ma (2σ) and 523.0 ± 4.2 Ma (2σ), respectively. A weighted mean age of 525.7 ± 2.3 Ma (2σ) was calculated for these two steps, within uncertainty of the plateau age of 528.5 ± 2.2 Ma (2σ) from grain 1.

Interpretation of age data

The weighted mean ^{40}Ar/^{39}Ar ages for phlogopite (526.9 ± 1.2 Ma [2σ]; 526.5 ± 2.0 Ma [2σ]) and the U-Pb perovskite age (512 ± 13 Ma [2σ]) for K1 D104 are statistically indistinguishable, adding confidence to the results from these two techniques. However, these ages are significantly younger than the Rb-Sr age of 565.4 ± 2.9 (Ma) calculated for phlogopite from the same sample. Decreasing apparent ^{40}Ar/^{39}Ar ages calculated for lower- to intermediate-temperature heating steps of sample K1 D104 suggest alteration of phlogopite (e.g., Phillips et al., 1999), a possibility that is supported by petrographic observations. This is an important observation, as alteration of phlogopite would perturb the Rb-Sr system, rendering the Rb-Sr age determination for K1 D104 unreliable. Thus, the statistically indistinguishable ^{40}Ar/^{39}Ar phlogopite ages and U-Pb perovskite age are considered more reliable determinations of the emplacement age for sample K1 D104 than the Rb-Sr age.

The high-precision ^{40}Ar/^{39}Ar plateau age determined for phlogopite from K1 D027 (528.5 ± 2.2 Ma [2σ]) is statistically indistinguishable from both the Rb-Sr age (528.6 ± 3.5 Ma [2σ]) calculated for this sample and the U-Pb and ^{40}Ar/^{39}Ar ages determined for K1 D104.

Using the upper and lower 2σ bounds as constraints, the Rb-Sr age determined for K2 D083 appears significantly older (+6.4 to +23.6 Ma) than those calculated for both K1 D027 and K1 D104. However, this age remains unconfirmed via alternative methods and is considered of low reliability, especially given the anomalously old Rb-Sr age calculated for K1 D104.

Discussion

The internal geology, surrounding structural geology, and apparent ages for the kimberlite pipes and dikes at Murowa provide some constraints on their timing and style of emplacement. In this section, we discuss factors which contribute to the textural, structural, and temporal complexity summarized above. The structural and geologic models are combined with radiometric dating of the Murowa pipes to build upon previous interpretations (Smith et al., 2004; Moss et al., 2013) of the style and history of kimberlite emplacement.

Kimberlite geology and metasomatism

The interpretations above imply that emplacement at the K1 and K2 pipes at Murowa record intermittent subvolcanic explosion and emplacement events occurring over a relatively extensive time period and likely involved compositionally and temporally distinct kimberlite fluids/magmas. In both K1 and K2, early and widespread metasomatism, dike intrusions, and local fluidization events were supplanted by more focused explosive events (e.g., pipe excavation at K2; emplacement of volcaniclastic rocks at K1), followed shortly thereafter by passive intrusions of coherent rocks within the pipes (Moss et al., 2013), in turn followed by the passive emplacement of cross-cutting planar dikes after the lithification of rocks derived from previous emplacement events.

Such widespread metasomatism and/or fracturing and brecciation of country rock is a feature which is well documented among kimberlites (Clement, 1982; Hetman et al., 2004; Mitchell et al., 2009; Kupsch and Armstrong, 2013; Muntener and Smith, 2013) and is observed adjacent to subsurface lithic breccias of carbonatite or other ultramafic composition (Jaques et al., 1986; Tompkins, 1991; Smith et al., 2013), as well as in magmatic and/or hydrothermal breccia pipes related to other mineral deposits (Bryant, 1968; Sillitoe, 1985). However, there are few comments in the literature on the overall geometry and volume of the damage zone surrounding the volcanic breccia pipes or speculation on the relative amount of fluid responsible for such features.

The Murowa pipes are interpreted to have been subjected to >600 m of erosion (Smith et al., 2004), similar to that interpreted for other localities with a surrounding contact or marginal country-rock breccias (e.g., Clement, 1982; Muntener and Smith, 2013). Significant crustal erosion on cratons effectively removes the near-surface products of eruptive activity which disrupt relatively little country rock during ascent, and contributes to an overall biased record of kimberlite volcanism (Brown and Valentine, 2013). We suggest that the "damage zone" surrounding the Murowa kimberlites may be common to most if not all other intrusions of fluid-rich ultramafic magmas and is a feature which may extend to depths in the crust consistent with the onset of volatile exsolution, but is likely underrepresented in the rock record due to variations in exposure level. The ratio of pipe infill to the marginal pipe zone may be a first-order proxy for the ratio of volatiles to solids and melt and, by extension, the explosivity and duration of the kimberlite eruption(s) at that depth in the volcanic system (Moss et al., 2013) but is complicated by the erosion bias: the apparent ratio of "damage zone" to pipe infill may be more reflective of the depth of erosion than the absolute ratio of fluids to liquids and solids in the kimberlite magma.

The geometry of the separate marginal pipe zones at Murowa appear to be broadly aligned but cover scales which preclude the influence of a single structure, in contrast with enclosed pipe infills which exhibit more focused geometry closely aligned with local structure (e.g., Fig. 3). This relationship is apparent at other kimberlite localities (Kurszlaukis and Barnett, 2003; Muntener and Smith, 2013), suggesting the emplacement of fluids or fluid-rich magma may be less controlled by local structure than more melt and solid rich magmas.

Emplacement in tensile bridges

A local structural model for the Murowa area is interpreted on the basis of field evidence and implies a large composite weak zone comprising tensile cracking in two directions from contrasting regimes of regional crustal stress. The relationship of the morphologies and orientations of kimberlite dikes and pipes relative to the structural model suggests the kimberlite emplacement was controlled both directly and indirectly by local structure, an observation consistent with those of Barnett (2006) on the kimberlites within the nearby Limpopo mobile belt. The location of K2 adjacent to a shear fracture that is part of the Popoteke fracture system believed to have controlled emplacement of the 2.5 Ga Great Dyke (Fedo et al., 1995) implies that the magma forming K2 likely utilized preexisting structures rather than creating its own fracture network in the near-surface environment. This interpretation is further supported by a number of planar kimberlite dikes with sheared and slickensided contacts that are parallel to and, in some cases, intrude within structures occupied by silica-epidote-chlorite, phases that are observed within the north-northeast structure set throughout the Murowa area. However, most dikes at Murowa are parallel to the two possible σ_1 directions indicated by the structural model, suggesting that the emplacement of kimberlite was indirectly responding to either local-scale heterogeneities in stress orientation or local stress tensors which evolved through time within the Murowa area.

The presence of kimberlite in orientations consistent with both primary regional structures and interpreted derivative local stress tensors within the same kimberlite cluster (Figs. 2, 13) implies an additional influence on emplacement position by the nature of the kimberlite magma, independent of structure. Dikes are more likely to propagate their own structures if they are overpressured (i.e., gas rich) and greatly exceed the tensile strength of the host rock (Delaney et al., 1986; Barnett, 2006; Kavanagh and Sparks, 2011), and a dike propagating its own fracture will most likely form a shear fracture at an angle to the principal vector of compression (Mandl, 2005). A key observation is that the early dikes and the largest and most internally complex kimberlite pipe (K1) at Murowa are located far from regional structures in positions and orientations consistent with derivative local stress tensors. Conversely, late intrusions and passively emplaced pipes (e.g., K2) are closer to and in positions and orientations consistent with regional structures (Fig. 2) or are largely irregular and nondirectional and found in the areas of lowest horizontal mean stress, i.e., inside kimberlite pipes (e.g., K1-KIMB1).

Moss et al. (2013) suggested that the textures apparent in the rocks at Murowa indicated emplacement involved significant amounts of phase separation within the kimberlite magma as it ascended, leading to varying types of intrusion from fluid-rich and solid-poor kimberlitic liquids to gas-poor intrusions of kimberlite magma. We suggest here that the relative proportion of gas present in an ascending magma exerts a direct control on the location and orientations of kimberlite emplacement relative to preexisting structures. Gas-rich fluids (e.g., metasomatic fluids) and gas-rich magmas (e.g., early dikes) are more likely to be emplaced away from regional structures and may create and fill fracture systems coincident with derivative

local stress tensors (e.g., early dikes and metasomatism at K1), while gas-poor magmas may preferentially utilize preexisting structures (e.g., K2, late dikes). Furthermore, we suggest that multiple emplacement events of varying explosivity through time (e.g., K1 and K2; Moss et al., 2013) can lead to a local stress tensor that is constantly evolving, such that ascending kimberlite magmas could encounter very different stress regimes within apparent timescales of emplacement (>6.4 Ma) in a given kimberlite cluster, leading to variable orientations of dikes and multilobed kimberlite pipes.

Relative timing and duration of kimberlite volcanism at Murowa

The data reported here for the Murowa kimberlites suggest that they are of ages similar to those of the Venetia kimberlite cluster (519.2 ± 5.8 Ma; Allsopp et al., 1995; Phillips et al., 1999), Colossus (533 ± 5.6 Ma; Phillips et al., 1999), some of the Marnitz kimberlites (Mooikloof model age = 518 Ma; Barton and Smith, 1991; Phillips et al., 1999), and those reported from Sese (538 ± 11 Ma; Smith et al., 2004). This finding supports interpretations of increased mantle-sourced magmatism during a Cambrian crustal extension event from ~500 to ~530 Ma across both the Limpopo mobile belt (Fedo et al., 1995) and the adjoining Zimbabwe craton to the north (Barton and Burger, 1983), covering an area approximately 40,000 km^2 in size.

The complex margins and internal crosscutting relationships in K1 and K2 were previously interpreted to reflect a series of subvolcanic explosion and emplacement events that occurred over a relatively extensive time period (Moss et al., 2013). The most reliable ages determined from two samples from dikes associated with K1 are statistically indistinguishable across three different methods, supporting this interpretation. Only one method was used to determine the age of a dike associated with K2, and, given the perturbed Rb-Sr systematics inferred from the $^{40}Ar/^{39}Ar$ step-heating results for K1, it is possible this result may be spurious. However, if the age for K2 is taken at face value, the apparently different emplacement ages of an early dike at K1 and a late dike from K2 at Murowa reported here combined with internal crosscutting relationships suggest emplacement of kimberlite in the small area of the Murowa kimberlite cluster (~2.5 km^2) may have occurred in multiple pulses over a time period in excess of 6 m.y. Age dating of kimberlites within a given kimberlite field (5–100s km^2) shows ranges of ~30 m.y. (Heaman et al., 2004; Lockhart et al., 2004), but there are few localities with demonstrated statistically distinct age ranges for kimberlites in close (<2 km) proximity (e.g., ~6 m.y.; Kjaarsgard et al., 2009). The dates from K1 and K2 suggest emplacement at the scale of kimberlite clusters (2–10 km^2) may cover more significant time periods (>6.4–<23.6 Ma) than previously envisaged, though a higher confidence estimate of the age of K2 is required to confirm this possibility.

Current techniques for dating kimberlites require pristine, unaltered mineral grains (phlogopite or perovskite) to avoid disturbing Rb-Sr, U-Pb, or $^{40}Ar/^{39}Ar$ systematics (Phillips et al., 1999; Heaman, 2009). Because of the requirement for fresh material, many published dates derive from a single rock type (e.g., Creaser et al., 2004), typically rich in solidified kimberlite melt, so as to provide abundant fresh mineral grains (e.g., coherent kimberlite, hypabyssal kimberlite, or magma clast-rich volcaniclastic kimberlite). However, some kimberlite pipes are known to have complex internal geology deriving from multiple emplacement phases (e.g., Koala; Nowicki et al., 2004), but there are very few published geochronology studies involving multiple, well-constrained and crosscutting phases of kimberlite in a single pipe (e.g., Zonneveldt et al., 2004; Kjaarsgard et al., 2009). This highlights the possibility that many dates reported for kimberlite pipes determined from a single facies of kimberlite may not reflect the emplacement ages of other facies in the same kimberlite, particularly in clusters and/or fields with apparently broad ranges in age (e.g., 45–75 Ma at Ekati; Creaser et al., 2004), and thus may lead to spurious associations or groupings with other kimberlites.

Conclusions

The internal geology and surrounding structural geology for the K1, K2, and K3 kimberlite pipes at Murowa are briefly described and modeled in three dimensions. The multilobed K1 contains 12 rock types which collectively define a complex pipe comprising coherent and volcaniclastic kimberlite surrounded by kimberlite-poor, metasomatized country-rock granite breccias and volcaniclastic rocks. The less complex K2 pipe comprises five rock types and is dominantly infilled by massive coherent kimberlite. The K3 pipe is irregular in shape and the internal geology remains poorly defined, but shows broad features consistent with those observed in K1. At K1, the observed textures are interpreted to indicate that kimberlite magmas with different proportions of gas, liquid, and solid phases intruded/erupted through variable country-rock regimes over contrasting timescales. Structural observations are used to generate a structural model interpreting the emplacement of the Murowa kimberlites into a zone of weak horizontal stress defined by two sets of preexisting, near-surface structures at different orientations. Based on observations of the spatial position and crosscutting relationships of kimberlite facies at Murowa, we propose that the abundance of gas in ascending kimberlite magma influences the relative size of the damage zone surrounding a kimberlite pipe and can also determine whether kimberlite is emplaced along preexisting structures or creates and intrudes its own fracture network. A reproducible Cambrian age of ~526 Ma is determined for two coherent kimberlite dikes at K1. An older Rb-Sr model age of ~543 Ma is calculated for a single dike from K2, but this result is of limited reliability due to potential disturbance of the Rb-Sr system during phlogopite alteration. We highlight the possibility that many dates reported for a single facies from a given kimberlite may not be representative of other kimberlites within the same cluster or different emplacement events in the same kimberlite body.

Acknowledgments

The authors would like to thank Rio Tinto plc and RioZim for access to resources for this study and for permission to publish. Discussions with Ammiel Manyumbu, Carlton Muchechetere, David Eichenberg, Paul Agnew, Murray Rayner, Casey Hetman, Andy Davy, and Kimberley Webb have greatly benefited this project. The contributions of Lovemore Chimuka, Chris Smith, Keith Sims, and Rio Tinto Exploration were essential

in developing the preliminary geology models. The paper was greatly assisted by the help of Keith Sims, who provided many of the internal reports and structural data, and was also further assisted by constructive reviews from two anonymous reviewers.

REFERENCES

Allsopp, H., Smith, C., Seggie, A., Skinner, E., and Colgan, E., 1995, The emplacement age and geochemical character of the Venetia kimberlite bodies, Limpopo belt, northern Transvaal: South African Journal of Geology, v. 98, p. 239–244.

Barnett, W., 2006, The mechanics of kimberlite emplacement: KwaZulu-Natal, South Africa, University of KwaZulu Natal, 287 p.

Barnett, W., Jelsma, H., Watkeys, M., Freeman, L., and Bloem, A., 2013, How structure and stress influence kimberlite emplacement: Springer, Special Issue of the Journal of the Geological Society of India, Proceedings of 10th International Kimberlite Conference, v. 2, p. 51–65.

Barton, E., and Burger, A., 1983, Reconnaissance isotopic investigations in the Namaqua mobile belt and implications for Proterozoic crustal evolution-Upington geotraverse: Geological Society of South Africa, Special Publication, v. 10, p. 191.

Barton, E.S., and Smith, C.B., 1991, Rb-Sr age for sample 173/50/K14/16 (Marnitz-Mooikloof): Johannesburg, South Africa, University of Witwatersrand, Bernard Price Institute for Geophysical Research, Lab Report, 1 p.

Basson, I.J., and Viola, G., 2003, Structural overview of selected group II kimberlite dyke arrays in South Africa: Implications for kimberlite emplacement mechanisms: South African Journal of Geology, v. 106, p. 375–394.

Batumike, J., Griffin, W., Belousova, E., Pearson, N., O'Reilly, S.Y., and Shee, S., 2008, LAM-ICPMS U-Pb dating of kimberlitic perovskite: Eocene-Oligocene kimberlites from the Kundelungu Plateau, DR Congo: Earth and Planetary Science Letters, v. 267, p. 609–619.

Bickle, M., Nisbet, E., and Martin, A., 1994, Archean greenstone belts are not oceanic crust: Journal of Geology, v. 102, p. 121–137.

Brown, R.J., and Valentine, G.A., 2013, Physical characteristics of kimberlite and basaltic intraplate volcanism and implications of a biased kimberlite record: Geological Society of America Bulletin, v. 125, p. 1224–1238.

Bryant, D.G., 1968, Intrusive breccias associated with ore, Warren (Bisbee) mining district, Arizona: Economic Geology, v. 63, p. 1–12.

Bulanova, G.P., Smith, C.B., Pearson, D.G., Kohn, S.C., Davy, A.T., McKay, A., and Marks, A., 2018, Diamonds from the Murowa kimberlites: Formation within extremely depleted and metasomatized Zimbabwean peridotitic subcontinental mantle: Society of Economic Geologists, Special Publication 20, p. 425–451.

Clement, C.R., 1982, A comparative geological study of some major kimberlite pipes in the Northern Cape and Orange Free State: Unpublished Ph.D. thesis, University of Cape Town, 2 volumes, 432 p., 406 p.

Cloos, H., 1941, Bau und Tatigkeit von Tuffschloten. Untersuchengen and dem Schabischen Vulkan: Vulkanologie und Geologische Rundschau, v. 32, p. 709–800.

Cox, R.A., and Wilton, D.H., 2006, U-Pb dating of perovskite by LA-ICP-MS: An example from the Oka carbonatite, Quebec, Canada: Chemical Geology, v. 235, p. 21–32.

Creaser, R.A., Grutter, H., Carlson, J., and Crawford, B., 2004, Macrocrystal phlogopite Rb-Sr dates for the Ekati property kimberlites, Slave province, Canada: Evidence for multiple intrusive episodes in the Paleocene and Eocene: Lithos, v. 76, p. 399–414.

Deakin, A.S., and White, S.H., 1991, Shear zone control of alkali intrusives: Examples from Argyle, northwestern Australia and Yengema, Sierra Leone, West Africa, *in* Meyer, H.O.A., and Leonardos, O.H., eds., Diamonds: Characterization, genesis and exploration, v. 2: Proceedings from 5th International Kimberlite Conference, Araxa, Brazil, Feb. 1991, p. 251–257.

Delaney, P.T., Pollard, D.D., Ziony, J.I., and McKee, E.H., 1986, Field relations between dikes and joints: Emplacement processes and paleostress analysis: Journal of Geophysical Research: Solid Earth (1978–2012), v. 91, p. 4920–4938.

Fedo, C.M., Eriksson, K.A., and Blenkinsop, T.G., 1995, Geologic history of the Archean Buhwa greenstone belt and surrounding granite-gneiss terrane, Zimbabwe, with implications for the evolution of the Limpopo belt: Canadian Journal of Earth Sciences, v. 32, p. 1977–1990.

Field, M., Gibson, J.G., Wilkes, T.A., Gababotse, J., and Khutjwe, P., 1997, The geology of the Orapa A/K1 Kimberlite Botswana: Further insights into the emplacement of kimberlite pipes: Russian Geology and Geophysics, v. 38, p. 24–39.

Fitzgerald, C.E., Hetman, C.M., Lepine, I., Skelton, D.S., and McCandless, T.E., 2009, The internal geology and emplacement history of the Renard 2 kimberlite, Superior province, Quebec, Canada: Lithos, v. 112, p. 513–528, Supplement 1.

Gamond, J., 1987, Bridge structures as sense of displacement criteria in brittle fault zones: Journal of Structural Geology, v. 9, p. 609–620.

Hall, C.M., 2013, Direct measurement of recoil effects on $^{40}Ar/^{39}Ar$ standards: Geological Society, London, Special Publications, v. 378, p. SP378.7.

Harder, M., Nowicki, T., Hetman, C., Freeman, L., and Abedu, B., 2013, Geology and evaluation of the K2 Kimberlite, Koidu mine, Sierra Leone, West Africa: Springer, Special Issue of the Journal of the Geological Society of India, Proceedings of 10th International Kimberlite Conference, v. 2, p. 191–208.

Hawkesworth, C., Bickle, M., Gledhill, A., Wilson, J., and Orpen, J., 1979, A 2.9-by event in the Rhodesian Archaean: Earth and Planetary Science Letters, v. 43, p. 285–297.

Heaman, L.M., 2009, The application of U-Pb geochronology to mafic, ultramafic and alkaline rocks: An evaluation of three mineral standards: Chemical Geology, v. 261, p. 43–52.

Heaman, L.M., Kjarsgaard, B.A., and Creaser, R.A., 2004, The temporal evolution of North American kimberlites: Lithos, v. 76, p. 377–397.

Helmstaedt, H., 2018, Tectonic and structural controls on diamondiferous kimberlite and lamproite and their bearing on area selection for diamond exploration: Society of Economic Geologists, Special Publication 20, p. 1–48.

Hetman, C.H., Scott-Smith, B.H., Paul, J.L., and Winter, F., 2004, Geology of the Gahcho Kue' kimberlite pipes, NWT, Canada: Root to diatreme magmatic transition zones: Lithos, v. 76, p. 51–74.

Hofmann, A., Dirks, P.H., and Jelsma, H.A., 2001, Horizontal tectonic deformation geometries in a Late Archaean sedimentary sequence, Belingwe greenstone belt, Zimbabwe: Tectonics, v. 20, p. 909–932.

Jaques, A.L., Lewis, J.D., and Smith, C.B., 1986, The kimberlites and lamproites of Western Australia: Geological Survey of Western Australia, Bulletin 132, 268 p.

Jelsma, H.A., de Wit, M.J., Thiart, C., Dirks, P.H.G.M., Viola, G., Basson, I.J., and Anckar, E., 2004, Preferential distribution along transcontinental corridors of kimberlites and related rocks of Southern Africa: South African Journal of Geology, v. 107, p. 301–324.

Jourdan, F., Matzel, J.P., and Renne, P.R., 2007, ^{39}Ar and ^{37}Ar recoil loss during neutron irradiation of sanidine and plagioclase: Geochimica et Cosmochimica Acta, v. 71, p. 2791–2808.

Kamenetsky, V.S., Kamenetsky, M.B., Weiss, Y., Navon, O., Nielsen, T.F.D., and Mernagh, T.P., 2009, How unique is the Udachnaya-East kimberlite? Comparison with kimberlites from the Slave craton (Canada) and SW Greenland: Lithos, v. 112, p. 334–346.

Kavanagh, J., 2010, Ascent and emplacement of kimberlite magmas: Unpublished Ph.D. thesis, Bristol, UK, University of Bristol, 373 p.

Kavanagh, J., and Sparks, R.S.J., 2011, Insights of dyke emplacement mechanisms from detailed 3D dyke thickness datasets: Journal of the Geological Society, London, v. 168, p. 965–978.

Keep, F.E., Worst, B.G., Wilson, J.F., and Robertson, I.M.D., 1970, Geological map of the country south of Chibi: Rhodesia Geological Survey, scale 1: 150,000.

Kjarsgaard, B.A., Harvey, S., McClintock, M., Zonneveld, J.P., Du Plessis, P., McNeil, D., and Heaman, L., 2009, Geology of the Orion South kimberlite, Fort à la Corne, Canada: Lithos, v. 112, p. 600–617.

Kupsch, B., and Armstrong, J., 2013, Exploration and geology of the Qilalugaq kimberlites, Rae Isthmus, Nunavut, Canada: Springer, Special Issue of the Journal of the Geological Society of India, Proceedings of 10th International Kimberlite Conference, p. 67–78.

Kurszlaukis, S., and Barnett, W.P., 2003, Volcanological and structural aspects of the Venetia kimberlite cluster—a case study of South African kimberlite maar-diatreme volcanoes: South African Journal of Geology, v. 106, p. 165–192.

Li, Q.-L., Li, X.-H., Liu, Y., Wu, F.-Y., Yang, J.-H., and Mitchell, R., 2010, Precise U-Pb and Th-Pb age determination of kimberlitic perovskites by secondary ion mass spectrometry: Chemical Geology, v. 269, p. 396–405.

Lockhart, G., Grütter, H., and Carlson, J., 2004, Temporal, geomagnetic and related attributes of kimberlite magmatism at Ekati, Northwest Territories, Canada: Lithos, v. 77, p. 665–682.

Luais, B., and Hawkesworth, C.J., 1994, The generation of continental crust: An integrated study of crust-forming processes in the Archaean of Zimbabwe: Journal of Petrology, v. 35, p. 43–94.

Ludwig, K.R., 2012, User's manual for Isoplot 3.75. A geochronological Tool-Kit for Microsoft Excel: Berkeley, California, Berkeley Geochronology Center, Special Publication No. 5, p. 75.

Maas, R., Kamenetsky, M.B., Sobolev, A.V., Kamenetsky, V.S., and Sobolev, N.V., 2005, Sr, Nd, and Pb isotope evidence for a mantle origin of alkali chlorides and carbonates in the Udachnaya kimberlite, Siberia: Geology, v. 33, p. 549–552.

Mandl, G., 2005, Rock joints: Berlin, Springer-Verlag, 221 p.

Marten, B., 1999a, Structural setting of the V10 kimberlites, Zimbabwe: Rio Tinto, Unpublished Report, 15 p.

——1999b, Visit note to V10: Additional observations on structural setting: Unpublished Report, Rio Tinto, 12 p.

Mitchell, R.H., 1995, Kimberlites, orangeites and related rocks: New York, Plenum Press, 410 p.

Mitchell, R.H., Skinner, E.M.W., and Scott Smith, B.H., 2009, Tuffisitic kimberlites from the Wesselton mine, South Africa: Mineralogical characteristics relevant to their formation: Lithos, v. 112, p. 452–464.

Moss, S., Webb, K., Hetman, C., and Manyumbu, A., 2013, Geology of the K1 and K2 Kimberlite pipes at Murowa, Zimbabwe: Springer, Special Issue of the Journal of the Geological Society of India, Proceedings of 10th International Kimberlite Conference, v. 2, p. 35–50.

Muntener, C., and Smith, B.S., 2013, Economic geology of Renard 3, Quebec, Canada: A diamondiferous, multi-phase pipe infilled with hypabyssal and tuffisitic kimberlite: Springer, Special Issue of the Journal of the Geological Society of India, Proceedings of 10th International Kimberlite Conference, v. 2, p. 241–256.

Nier, A.O., 1950, A redetermination of the relative abundances of the isotopes of carbon, nitrogen, oxygen, argon, and potassium: Physical Review, v. 77, p. 789.

Nowicki, T., Crawford, B., Dyck, D., Carlson, J., McElroy, R., Oshust, P., and Helmstaedt, H., 2004, The geology of kimberlite pipes of the Ekati property, Northwest Territories, Canada: Lithos, v. 76, p. 1–27.

Odin, G. S., 1982, Numerical dating in stratigraphy: Chichester, John Wiley and Sons, 1040 p.

Paton, C., Hergt, J.M., Phillips, D., Woodhead, J.D., and Shee, S.R., 2007, New insights into the genesis of Indian kimberlites from the Dharwar craton via in situ Sr isotope analysis of groundmass perovskite: Geology, v. 35, p. 1011–1014.

Paton, C., Woodhead, J.D., Hellstrom, J.C., Hergt, J.M., Greig, A., and Maas, R., 2010, Improved laser ablation U-Pb zircon geochronology through robust downhole fractionation correction: Geochemistry, Geophysics, Geosystems, v. 11, 36 p.

Pearson, D.G., Liu, J., Smith, C.B., Mather, K.A., Krebs, M.Y., Bulanova, G.P., and Kobussen, A.F., 2018, Characteristics and origin of the mantle root beneath the Murowa diamond mine: Implications for craton and diamond formation: Society of Economic Geologists, Special Publication 20, p. 403–424.

Phillips, D., and Harris, J., 2009, Diamond provenance studies from $^{40}Ar/^{39}Ar$ dating of clinopyroxene inclusions: An example from the west coast of Namibia: Lithos, v. 112, p. 793–805.

Phillips, D., and Matchan, E., 2013, Ultra-high precision $^{40}Ar/^{39}Ar$ ages for Fish Canyon Tuff and Alder Creek Rhyolite sanidine: New dating standards required?: Geochimica et Cosmochimica Acta, v. 121, p. 229–239.

Phillips, D., Kiviets, G.B., Barton, E.S., Smith, C.B., Viljoen, K.S., and Fourie, L.F., 1999, $^{40}Ar/^{39}Ar$ dating of kimberlites and related rocks: Problems and solution, *in* Gurney, J.J., Gurney, J.L., Pascoe, M.D., and Richardson, S.H., eds., The Nixon Volume: Proceedings of the 7th International Kimberlite Conference, Cape Town, South Africa, 1999, p. 677–688.

Renne, P.R., Swisher, C.C., Deino, A.L., Karner, D.B., Owens, T.L., and DePaolo, D.J., 1998, Intercalibration of standards, absolute ages and uncertainties in $^{40}Ar/^{39}Ar$ dating: Chemical Geology, v. 145, p. 117–152.

Robertson, I.D., 1974, Explanation of the geological map of the country south of Chibi: Short: Republic of Zimbabwe Geological Survey, v. 41, p. 40.

Scott Smith, B., Nowicki, T., Russell, J., Webb, K., Mitchell, R., Hetman, C., Harder, M., Skinner, E., and Robey, J.A., 2013, Kimberlite terminology and classification: Special Issue of the Journal of the Geological Society of India, v. 2, p. 1–17.

Sillitoe, R.H., 1985, Ore-related breccias in volcanoplutonic arcs: Economic Geology, v. 80, p. 1467–1514.

Sims, K., Fox, K., Harris, M., Chimuka, L., Reichhardt, F., Muchemwa, E., Gowera, R., Hinks, D., and Smith, C.B., 2018, Discovery of the Murowa kimberlites, Zimbabwe: Society of Economic Geologists, Special Publication 20, p. 359–378.

Smith, C.B., 1983, Pb, Sr and Nd isotopic evidence for sources of southern African Cretaceous kimberlites: Nature, v. 304, p. 51–54.

Smith, C.B., Sims, K., Chimuka, L., Duffin, A., Beard, A.D., and Townend, R., 2004, Kimberlite metasomatism at Murowa and Sese pipes, Zimbabwe: Lithos, v. 76, p. 219–232.

Smith, C., Haggerty, S., Chatterjee, B., Beard, A., and Townend, R., 2013, Kimberlite, lamproite, ultramafic lamprophyre, and carbonatite relationships on the Dharwar craton, India; an example from the Khaderpet pipe, a diamondiferous ultramafic with associated carbonatite intrusion: Lithos, v. 182, p. 102–113.

Soederlund, U., Hofmann, A., Klausen, M.B., Olsson, J.R., Ernst, R.E., and Persson, P.O., 2010, Towards a complete magmatic barcode for the Zimbabwe craton: Baddeleyite U-Pb dating of regional dolerite dyke swarms and sill complexes: Precambrian Research, v. 183, p. 388–398.

Spell, T.L., and McDougall, I., 2003, Characterization and calibration of $^{40}Ar/^{39}Ar$ dating standards: Chemical Geology, v. 198, p. 189–211.

Steiger, R.H., and Jäger, E., 1977, Subcommission on geochronology: Convention on the use of decay constants in geo- and cosmochronology: Earth and Planetary Science Letters, v. 36, p. 359–362.

Tappe, S., and Simonetti, A., 2012, Combined U-Pb geochronology and Sr-Nd isotope analysis of the Ice River perovskite standard, with implications for kimberlite and alkaline rock petrogenesis: Chemical Geology, v. 304, p. 10–17.

Tompkins, L., 1991, The Japecanga pipe: Geological Survey of Brazil (CPRM) Field Guidebook, Fifth International Kimberlite Conference, CPRM Special Publication, p. 45–48.

White, S., De Boorder, H., and Smith, C., 1995, Structural controls of kimberlite and lamproite emplacement: Journal of Geochemical Exploration, v. 53, p. 245–264.

Wiedenbeck, M., Alle, P., Corfu, F., Griffin, W., Meier, M., Oberli, F., von Quadt, A., Roddick, J., and Spiegel, W., 1995, Three natural zircon standards for U-Th-Pb, Lu-Hf, trace element and REE analyses: Geostandards Newsletter, v. 19, p. 1–23.

Wilson, J., 1990, A craton and its cracks: Some of the behaviour of the Zimbabwe block from the Late Archaean to the Mesozoic in response to horizontal movements, and the significance of some of its mafic dyke fracture patterns: Journal of African Earth Sciences (and the Middle East), v. 10, p. 483–501.

Woodhead, J., Hergt, J., Shelley, M., Eggins, S., and Kemp, R., 2004, Zircon Hf-isotope analysis with an excimer laser, depth profiling, ablation of complex geometries, and concomitant age estimation: Chemical Geology, v. 209, p. 121–135.

Wu, F.-Y., Yang, Y.-H., Mitchell, R.H., Li, Q.-L., Yang, J.-H., and Zhang, Y.-B., 2010, In situ U-Pb age determination and Nd isotopic analysis of perovskites from kimberlites in southern Africa and Somerset Island, Canada: Lithos, v. 115, p. 205–222.

Zonneveld, J.-P., Kjarsgaard, B.A., Harvey, S.E., Heaman, L.M., McNeil, D.H., and Marcia, K.Y., 2004, Sedimentologic and stratigraphic constraints on emplacement of the Star Kimberlite, east-central Saskatchewan: Lithos, v. 76, p. 115–138.